Chemical Geology 425 (2016) 12–36

Contents lists available at ScienceDirect

Chemical Geology

journal homepage: www.elsevier.com/locate/chemgeo

Invited Review Article

The continental Si cycle and its impact on the ocean Si isotope budget

Patrick J. Frings *, Wim Clymans, Guillaume Fontorbe, Christina L. De La Rocha, Daniel J. Conley

Department of Geology, Lund University, Sweden

ARTICLE INFO

Article history:
Received 16 July 2015
Received in revised form 5 January 2016
Accepted 24 January 2016
Available online 28 January 2016

Keywords:
Global silicon cycle
Biogenic silica
Silicon isotopes
LGM
Palaeoceanography
Biogeochemical cycling

ABSTRACT

The silicon isotope composition of biogenic silica ($\delta^{30}Si_{BSi}$) in the ocean is a function of the $\delta^{30}Si$ of the available dissolved Si (DSi; H_2SiO_4), the degree of utilisation of the available DSi, and, for some organisms, the concentration of DSi. This makes $\delta^{30}Si_{BSi}$ in sediment archives a promising proxy for past DSi concentrations and utilisation. At steady-state, mean $\delta^{30}Si_{BSi}$ must equal a weighted average of the inputs, the majority of which are of continental origin. Variation in the functioning of the continental Si cycle on timescales similar to the residence time of DSi in the ocean (~10 ka) may therefore contribute to downcore variability in $\delta^{30}Si_{BSi}$ on millennial or longer timescales. The direction and magnitude of change in published $\delta^{30}Si_{BSi}$ records over the last few glacial cycles is consistent among ocean basins and between groups of silicifiers. They document glacial values that are typically 0.5 to 1.0‰ lower than interglacial values and together hint at coherent and predictable glacial–interglacial variability in whole-ocean $\delta^{30}Si$ driven by a change in mean $\delta^{30}Si$ of the inputs. In this contribution, we review the modern inputs of DSi to the ocean and the controls on their isotopic composition, and assess the evidence for their variability on millennial-plus timescales.

Today, 9.55×10^{12} mol yr^{-1} DSi enters the ocean, of which roughly 64% and 25% are direct riverine inputs of DSi, and DSi from dissolution of aeolian and riverborne sediment, respectively. The remainder derives from alteration or weathering of the ocean crust. Each input has a characteristic $\delta^{30}Si$, with our current best estimate for a weighted mean being 0.74‰, although much work remains to be done to characterise the individual fluxes. Many aspects of the continental Si cycle may have differed during glacial periods that together can cumulatively substantially lower the mean $\delta^{30}Si$ of DSi entering the ocean. These changes relate to i) a cooler, drier glacial climate, ii) lowered sea level and the exposure of continental shelves, iii) the presence of large continental ice-sheets, and iv) altered vegetation zonation.

Using a simple box-model with a Monte-Carlo approach to parameterisation, we find that a transition from a hypothesised glacial continental Si cycle to the modern Si cycle can drive an increase in whole ocean $\delta^{30}Si$ of comparable rate and magnitude to that recorded in $\delta^{30}Si_{BSi}$. This implies that we may need to revisit our understanding of aspects of the Si cycle in the glacial ocean. Although we focus on the transition from the last glacial, our synthesis suggests that the continental Si cycle should be seen as a potential contributory factor to any variability observed in ocean $\delta^{30}Si_{BSi}$ on millennial or longer timescales.

Contents

* Corresponding author.

http://dx.doi.org/10.1016/j.chemgeo.2016.01.020

1. Introduction

At or near the Earth's surface silicate minerals can be chemically weathered, a process that forms soils, releases solutes and ultimately sustains life. The solutes that are released, including dissolved Si ($Si(OH)_4$; hereafter DSi), enter biogeochemical cycles – the movement of elements through the environment – that end with burial in marine sediments. The global Si cycle is characterised by one relatively discrete sub-cycle on the continents and another in the oceans (Fig. 1). The transfer of Si between the two is essentially unidirectional, so the land-to-ocean Si flux is of interest both as an integrative function of the continental Si cycle and as the chief input for the ocean Si cycle. The purpose of this contribution is (i) to review the fluxes of Si from land to ocean and the mechanisms that determine their magnitude and silicon isotopic composition (δ^{30}Si), (ii) to estimate plausible limits on the magnitude by which these fluxes can vary on millennial or longer timescales, and (iii) to assess the extent to which this variability is propagated to the ocean Si cycle and is visible in palaeoenvironmental archives.

Besides silicon's inherent interest as a major and ubiquitous element, two reasons for studying the Si cycle are commonly put forward. First, the process of chemical weathering of silicate minerals is a key step in the sequestration of atmospheric CO_2 as marine carbonates and hence is a key term in the long-term ('geological') carbon cycle (Walker et al., 1981). The rate of silicate weathering should be related to the concentration of atmospheric CO_2, *via* climatological and biological feedbacks in order to provide the negative feedback necessary to balance the continuous carbon degassing from the solid earth (Berner and Caldeira, 1997). Therefore, understanding the global Si cycle can provide insight to the functioning of Earth's thermostat. Second, DSi is a nutrient for many organisms. For some – notably the diatoms (class: Bacillariophyceae) – it is an essential nutrient. For others, including many vascular plants, DSi provides ecological, physiological or structural benefits (Epstein, 1999; Guntzer et al., 2012; Pilon-Smits et al., 2009). The availability of DSi in aquatic ecosystems controls the amount of siliceous primary productivity (mostly diatoms, which today account for 40% of ocean primary productivity) (Egge and Asknes, 1992). This siliceous production is also a key component of the ocean biological pump, which determines the partitioning of carbon between the deep ocean and the atmosphere on centennial to millennial timescales (De La Rocha, 2006).

This contribution builds on earlier reviews that have explored either the ocean Si budget, but without consideration of a Si isotope perspective (Tréguer et al., 1995; Tréguer and De La Rocha, 2013), or the continental Si isotope cycle (Opfergelt and Delmelle, 2012). It is partly motivated by the proliferation of marine biogenic silica δ^{30}Si records that are conventionally interpreted in terms of palaeonutrient utilisation or water-mass mixing (see Section 2.3). Here, we use our synthesis to advance the hypothesis that these δ^{30}Si records may also reflect changes in the continental Si cycle. This review is structured as follows: first, we provide basic background information on the continental Si cycle (Section 2.1), silicon isotope geochemistry (Section 2.2), and the use and conventional interpretation of downcore fluctuations in δ^{30}Si in marine sediments as a palaeoenvironmental proxy on millennial-plus timescales (Section 2.3). Section 3 summarises the controls on the silicon isotope composition of continental waters. We then report the current state-of-the-art of DSi inputs to the global ocean on a flux-by-flux basis (Section 4), paying close attention to the δ^{30}Si of these

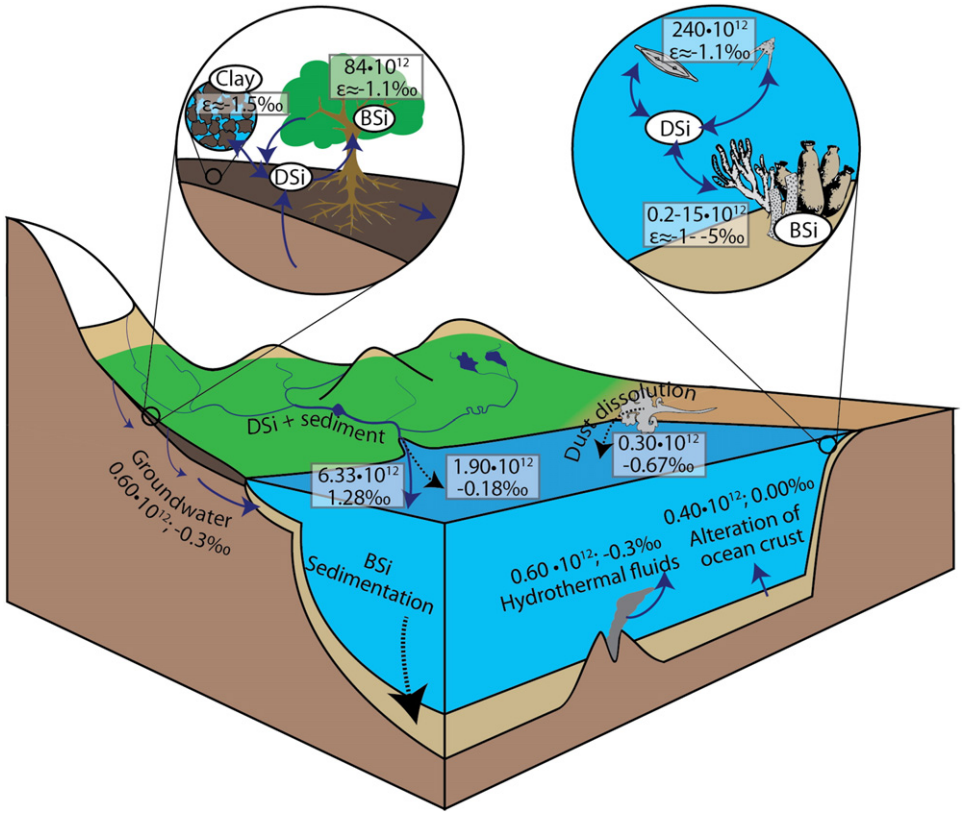

Fig. 1. Cartoon schematic of the modern day global Si cycle. The values show the magnitudes of the fluxes (in 10^{12} mol yr^{-1}) and their associated δ^{30}Si values (in ‰). Typical fractionations (ε, ‰) associated with production of biogenic silica (BSi) and clay minerals are shown in the inset panels. Dotted lines indicate particulate fluxes; solid lines indicate solute fluxes or transformations. See main text for details.

fluxes. In Section 5, we consider how these fluxes may vary on millennial-plus timescales. Finally, in Section 6, we use a simple box-modelling approach to exploit our synthesis and assess what these variations could mean for the ocean Si cycle, and how this may be recorded in palaeoenvironmental archives.

2. Background

2.1. The continental Si cycle

The key processes in the continental Si cycle are schematised in Fig. 1, and have been reviewed in detail elsewhere (Cornelis et al., 2011). The cycle begins with the release of dissolved silica (DSi) during weathering processes. A fraction may then be transferred directly to the fluvial system, *via* groundwater or soil water flow. A fraction may be incorporated into, or adsorbed onto, secondary phases of variable stability. Finally, a fraction may be utilised by vascular plants that take up DSi and subsequently precipitate it as biogenic silica (BSi) structures termed phytoliths (Carey and Fulweiler, 2012; Massey et al., 2006; Piperno, 2001). Upon litterfall the BSi returns to the soil where it may dissolve, be stored, or be structurally or chemically altered (Barão et al., 2014; Sommer et al., 2006). Ultimately, Si will be lost to the fluvial system as both DSi and eroded particulate Si. BSi, altered BSi and pedogenic silicates can have similar solubilities and reactivities, so the term 'amorphous silica' (ASi) is commonly used instead (Saccone et al., 2007). The net result of continental Si cycling is that in many ecosystems, a soil–plant ASi pool develops that is orders of magnitude larger than the annual release of DSi from primary minerals *via* weathering (Blecker et al., 2006; Clymans et al., 2011; Struyf et al., 2010a). Because of this, it is conceptualised that terrestrial soil–plant systems buffer the release of Si from the continents, at least in some settings (Struyf and Conley, 2012), and that perhaps even a majority of river DSi passes through this buffer before export into the river system (Derry et al., 2005; Struyf et al., 2009). Once in the river system, both biotic and abiotic processes can further modify the Si flux. Lakes and reservoirs provide low-turbidity environments particularly conducive to BSi production by diatoms (Frings et al., 2014a; Lauerwald et al., 2013). In-stream processes and the functioning of floodplains and hyporheic and riparian zones may also be important (Bouwman et al., 2013). Estuaries and deltas constitute a final zone with the capacity to modify river Si fluxes (Milliman and Boyle, 1975; Conley and Malone, 1992; Weiss et al., 2015).

2.2. Low temperature silicon isotope geochemistry

There are three naturally occurring stable isotopes of Si: ^{28}Si, ^{29}Si and ^{30}Si, with atomic masses of 27.97693, 28.97649 and 29.97377 and relative abundances of *ca.* 92.2%, 4.7% and 3.1%, respectively (Ding et al., 2005a). They fractionate during almost all of the low-temperature processes that define the continental and oceanic Si cycles, making them a useful geochemical tracer.

Variations in silicon stable isotope abundances are presented in delta notation as δ^{29}Si or δ^{30}Si, *i.e.* the deviation in parts per thousand of a given isotope ratio (^{29}Si/^{28}Si or ^{30}Si/^{28}Si, respectively) from the same ratio in a standard reference material. For Si, this reference material is quartz grains known as NBS28 (RM 8546), and is distributed by the National Institute of Standards (NIST). The isotopic composition (δ^{30}Si, in per mil) of a sample is then:

$$\delta^{x}\mathrm{Si} = \left[{}^{R_{sample}}\!/_{R_{standard}} - 1 \right] \times 1000 \quad (1)$$

where R is the ratio of ^{x}Si/^{28}Si in the sample and standard, and x is 29 or 30. Differences in Si isotopic composition between two phases can be

caused by isotope fractionation, a process that stems from differences in the masses of the isotopes. Fractionation can result from either kinetic or equilibrium isotope effects and the fractionation of initial (substrate) phase A relative to product phase B is termed the fractionation factor, α:

$$^{x}\alpha_{A-B} = {}^{R_A}/_{R_B}. \quad (2)$$

For Si, α_{A-B} is typically very close to one, and so is also presented in permil as ε:

$$^{x}\varepsilon_{A-B} = 10^3(^{x}\alpha_{A-B}-1). \quad (3)$$

Both kinetic and equilibrium isotope effects stem from mass dependent fractionation, and therefore a plot of δ^{30}Si against δ^{29}Si defines a predictable relationship that is a function of the mass-dependence of the fractionation factors (Young et al., 2002): $^{29}\alpha_{A-B} = (^{30}\alpha_{A-B})^{\beta}$ where β for atomic Si is 0.5092 for kinetic fractionation and 0.5178 for equilibrium fractionation. Generally, kinetic isotope fractionation occurs when the chemical reaction or mass-transfer is unidirectional, and preferentially enriches the product in lighter isotopes. Equilibrium isotope fractionation occurs when chemical reactions are at equilibrium, and tends to partition the heavier isotopes into the phase with a lower energy state. Given the relatively small range of Si isotope fractionations observed at the Earth's surface, the two are essentially indistinguishable at current measurement precision. Deviations from mass-dependency implies mass-independent isotope fractionation, unknown for silicon isotopes during Earth surface processes, so adherence to mass-dependent fractionation is instead more commonly used as an indicator of the successful removal of interferences during measurement.

Some generalisations can be made about the nature of silicon isotope fractionations in the low-temperature environments that characterise the Earth's surface. The tendency is for fractionation associated with the formation of a solid from a solution to favour the incorporation of the lighter isotopes into the new solid, leaving the residual solution enriched in the heavier isotopes (*i.e.* kinetic, not equilibrium isotope fractionations appear to predominate) (De La Rocha et al., 1997, 2000; Opfergelt and Delmelle, 2012; Ziegler et al., 2005a,b). In other words, $\varepsilon_{A-B}<0$ or $\alpha_{A-B}<1$, and is observed in the formation of BSi by diatoms, sponges, radiolarians and plants, and in the formation of secondary minerals (Fig. 2).

Two simple models are commonly used to predict and interpret the evolution of silicon isotope compositions as a function of f_{Si}, the fraction of the available Si in reactant A converted or transferred to product B, with an associated permil enrichment ε_{A-B}. The first model describes the evolution of δ^{30}Si in the reactant and product when a finite-pool of reactant is isolated from fresh sources of Si, and the products do not interact further. In this case, both the residual pool of reactant Si and the pool of produced Si define Rayleigh distillation curves, where the accumulated product, $\delta^{30}Si_B$, is given by:

$$\delta^{30}Si_B = \delta^{30}Si_{A,0} - \left({}^{f_{Si}}/_{1-f_{Si}}\right)\cdot\varepsilon^{30}_{A-B}\cdot\ln(f_{Si}) \quad (4)$$

and the residual reactant, $\delta^{30}Si_A$, is given by:

$$\delta^{30}Si_A = \varepsilon^{30}_{A-B}\cdot\ln(f_{Si}) \quad (5)$$

where $\delta^{30}Si_{A,0}$ is the isotopic composition of the source Si at time 0 (Mariotti et al., 1981). An alternative model describes the evolution of δ^{30}Si when the production of pool B is at a steady-state with a constant supply of fresh reactant into the system:

$$\delta^{30}Si_B = \delta^{30}Si_{A,0} + \varepsilon^{30}_{A-B}\cdot f_{Si} \quad (6)$$

with the residual reactant Si simply being:

$$\delta^{30}Si_A = \varepsilon^{30}_{A-B}(1-f_{Si}). \quad (7)$$

Eqs. (6) and (7) also apply to a system with a finite pool of Si, in which the reactant and products interact and partition according to f_{Si}. Both models are shown graphically in Fig. 3. The terms 'open' and 'closed' models have been applied to both models, depending on whether the perspective of the reactant or product is taken, and whether the reaction is considered unidirectional or not. For clarity, we refer to the first model (Eqs. (4) and (5)) as a Rayleigh model and the second (Eqs. (6) and (7)) as a steady-state model.

At least 1500 δ^{30}Si determinations, summarised in Fig. 4, have been made on continental material alone, and a similar number on oceanic and extra-terrestrial material. The range of fractionations during low-temperature processes is sufficient to imprint measurable, interpretable and in some cases distinctive δ^{30}Si values on to natural Si bearing phases (Fig. 4). Essentially, this means the stable isotopes of silicon can provide information on Si sources and processes above and beyond that available from simple mass-balance considerations. In this manuscript all

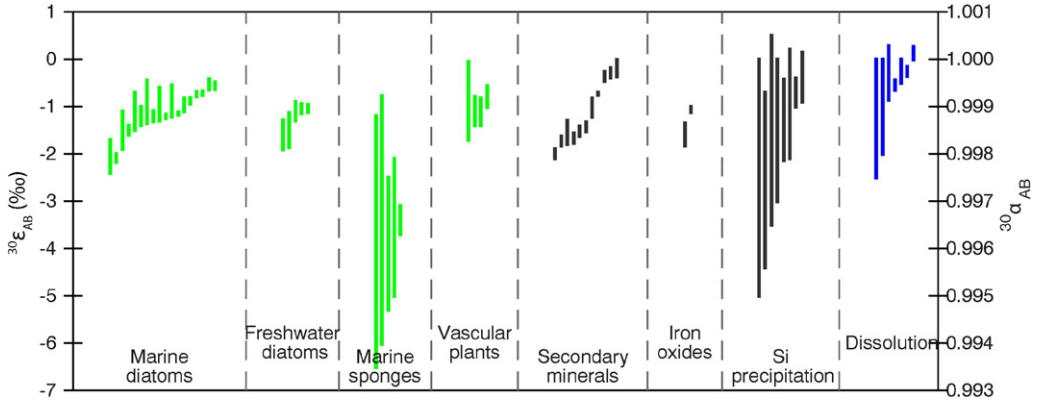

Fig. 2. Summary of published estimates of fractionations associated with the biological or geochemical cycling of Si at the Earth's surface. All fractionations refer to a transformation between a solid phase (product) and a dissolved phase (reactant); the bars represent the range observed in each work. Estimates were obtained from the following sources: *Marine diatoms*: De La Rocha et al. (1997), Sutton et al. (2013), Varela et al. (2004), Cardinal et al. (2005), Reynolds et al. (2006), Beucher et al. (2008), Fripiat et al. (2011), Milligan et al. (2004), De La Rocha et al. (2011), and Egan et al. (2012). *Freshwater (and estuarine) diatoms*: Alleman et al. (2005), Opfergelt et al. (2011), Sun et al. (2013, 2014), and Panizzo et al. (2016). *Marine siliceous sponges*: Hendry and Robinson (2012), Hendry et al. (2010), Wille et al. (2010), and Douthitt (1982). *Vascular plants*: Ding et al. (2005b, 2008), Opfergelt et al. (2006), and Ziegler et al. (2005b). *Secondary minerals*: Ziegler et al. (2005b), Georg et al. (2007a, 2009b), Opfergelt et al. (2010, 2011, 2012), and Basile-Doelsch et al. (2005). *Iron oxides*: Delstanche et al. (2009). *(A)Si precipitation*: Geilert et al. (2014, 2015), Oelze et al. (2014, 2015), Roerdink et al. (2015), Ding et al. (2008), Ziegler et al. (2005a), and Li et al. (1995). *Dissolution*: Ziegler et al. (2005a), Frings et al. (2014c), Demarest et al. (2009), Wetzel et al. (2014), and Sun et al. (2014).

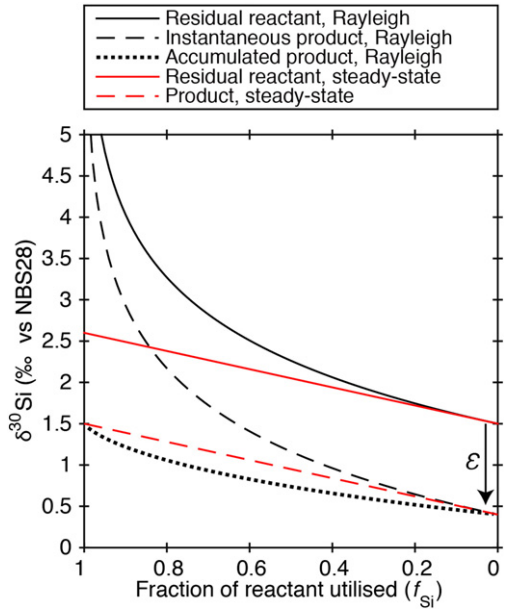

Fig. 3. Schematic showing the evolution of δ^{30}Si in two fractionation models as Si is converted from one phase to another with an associated fractionation ε. Red lines display the case when there is a steady supply of fresh reactant into the system (with constant δ^{30}Si), *i.e.* the steady-state model. Black lines display the case when there is a finite pool of reactant being converted into a product that has no further interaction, *i.e.* the Rayleigh model. Solid lines indicate the isotopic evolution of the reactant, dashed lines the evolution of the instantaneous product, which is always reactant + ε. The dotted line represents the accumulated (integrated) product of a Rayleigh fractionation model. At $f_{Si} = 1$, all reactant is converted to product, so the product has the composition of the initial solution.

silicon isotope ratios are presented as δ^{30}Si relative to NBS28, and corrected where necessary from published δ^{29}Si values assuming a mass-dependency factor of 0.51 (see above). The first measurements were reported relative to the Caltech Rose Quartz Standard (RQS) (*e.g.* Douthitt, 1982), which should produce roughly comparable results since NBS28 and RQS apparently have near-identical Si isotope ratios (Georg et al., 2007b). Early measurements used gas-source mass spectrometers after fluorination of Si to the gaseous SiF_4 (*e.g.* Reynolds and Verhoogen, 1953), but the use of multi-collector inductively-coupled-plasma mass-spectrometry (MC-ICP-MS) is becoming increasingly dominant and can achieve <0.1‰ 2σ external reproducibility (*e.g.* Zambardi and Poitrasson, 2011). The use of a laser-ablation unit attached to a MC-ICP-MS (*e.g.* Steinhoefel et al., 2011) or of secondary ion mass-spectrometry (*e.g.* Basile-Doelsch et al., 2005) are also becoming more prevalent and offer the advantages of in-situ analysis, though they have not reached the precision of solution MC-ICP-MS.

2.3. Silicon isotopes in marine biogenic silica as a palaeoenvironmental proxy

The δ^{30}Si of biosiliceous remains in marine sediments is being increasingly used as a palaeoceanographic tool (De La Rocha et al., 1998; Hendry et al., 2014). There has been a particular focus on the transition from the last glacial maximum (LGM, *ca.* 21 ka) to the present day and to date, δ^{30}Si records have been developed from diatoms, sponges or radiolarians from at least 21 cores over the deglacial period (Fig. 5). These records are globally distributed, although more prevalent in the Southern Ocean which plays a large role in the modern day marine silica cycle and where sediments of more than 85 wt.% biogenic silica may be found. They are not straightforward to interpret. The modern day silicon isotope distribution reflects an interplay between biogenic silica production and dissolution, and the physical mixing of the ocean (de Souza et al., 2012, 2014; Reynolds, 2009; Wischmeyer et al., 2003). Together, these combine to produce water masses with relatively distinct DSi concentrations and δ^{30}Si. Deconvolving the effects of one from the other, even when assuming preservational or species-specific biases (vital effects) are negligible (Sutton et al., 2013), becomes tricky.

A conventional interpretation considers changes in δ^{30}Si of surface-dwelling organisms (diatoms and radiolarians) as reflecting DSi utilisation (De La Rocha et al., 1998; Maier et al., 2013). By considering the pool of DSi from which diatoms and radiolarians precipitate their skeletons as either a finite pool which is not immediately replenished (*i.e.* bloom conditions) or a continuously replenished pool (*i.e.* non-bloom conditions), it is possible to relate the δ^{30}Si of the product (*i.e.* the BSi) to f_{Si}, the fraction of DSi utilised (Section 2; Fig. 3), assuming $\varepsilon_{DSi-BSi}$ and initial δ^{30}Si are known. The interpretation is different for siliceous sponges, benthic animals partly comprising the phylum Porifera, that produce skeletons of biogenic silica. The fractionation of silicon isotopes (approximated as the difference between DSi and sponge δ^{30}Si, *i.e.* $\Delta\delta^{30}$Si) by sponges varies as a function of $[DSi]^{-1}$, increasing to an observed maximum magnitude of ${}^{30}\varepsilon_{DSi-BSi} \approx -5‰$ at high (>100 μM) concentrations (Hendry and Robinson, 2012; Wille et al., 2010). Changing δ^{30}Si of sponge-spicule BSi therefore reflects changes in either ambient DSi concentrations or the isotopic composition of the DSi, or both.

Given that the Si isotope fractionation associated with diatom BSi production is around −1.1‰ (De La Rocha et al., 1997; Sun et al., 2014; Sutton et al., 2013), then large changes in f_{Si} are required to explain the downcore shifts greater than a few tenths of a permil in diatom δ^{30}Si records, assuming initial δ^{30}Si remains constant, independent of the model chosen. For example, if the entirety of the change in diatom δ^{30}Si observed in core MD88-769 (from +1.02‰ to +1.99‰) (Beucher et al., 2007) is attributable to variable palaeoutilisation of DSi, this implies a shift from near-zero DSi usage to near-complete utilisation, assuming a constant diatom fractionation of −1.1‰ (see Fig. 5). These extreme changes strongly suggest other processes must be involved. There is therefore a growing awareness that downcore diatom δ^{30}Si records can also partly reflect *e.g.* species specific effects (Sutton et al., 2013), water mass mixing or circulation (*e.g.* Beucher et al., 2007) or a whole-ocean change in δ^{30}Si of DSi (the hypothesis advanced here).

The published marine BSi δ^{30}Si records, summarised in Fig. 5, show a general increase in δ^{30}Si from the LGM to the present day superimposed on higher frequency variability. These typically exhibit total variability of 0.5–1.0‰. This pattern of lower glacial δ^{30}Si to higher interglacial δ^{30}Si is well recognised and has been documented in the Southern Ocean (De La Rocha et al., 1998; Horn et al., 2011), the eastern equatorial Pacific (Pichevin et al., 2009) and the north Atlantic (Hendry et al., 2014), and has also been shown to be a feature of previous glacial–interglacial cycles (Brzezinski et al., 2002; Ellwood et al., 2010; Griffiths et al., 2013). It also appears to be consistent between benthic and planktic organisms. Given this consistency among ocean-basins, different silicifying organisms, and repeatability across different glacial cycles, coupled with the large changes in DSi utilisation implied (see above), this raises the question to what extent these changes reflect a whole-ocean shift rather than local shifts in palaeoproductivity or nutrient utilisation.

3. What controls δ^{30}Si of DSi in continental waters?

Many hundreds of individual DSi–δ^{30}Si determinations from rivers, soil waters, lakes and groundwaters are now available (Fig. 4). This allows a number of results to be generalised:

- River water DSi–δ^{30}Si is higher than the minerals from which it ultimately derives.
- There is no global relationship between δ^{30}Si and DSi concentrations (Fig. 6a) (or DSi fluxes where available; Fig. 6b): both positive and negative correlations have been reported from individual systems.
- There is no relationship between δ^{30}Si and latitude (Fig. 6c).

- Individual sampling stations tend to show seasonal variability of *ca.* 0.5‰ to 1.0‰ with lower values corresponding to high-discharge periods (Fig. 6d).
- River δ^{30}Si tends to increase downstream (Fig. 7).

As a first step, we can probably discount variability inherited directly from the various groups of minerals that collectively constitute 'bedrock.' Although these do exhibit some variability, in particular in shales and other sedimentary rocks (Douthitt, 1982; Savage et al., 2013), they tend to define a limited range of silicon isotope compositions around an upper crustal average of *ca.* −0.25‰ (Fig. 4). Compared to this, the range of values observed in river waters (almost 5‰) is too large to have been imparted from source material variability. We can probably also discount silicon isotope fractionation during the initial solubilisation of Si from the parent material. While a series of dissolution experiments with Hawaiian basalts has demonstrated the preferential initial release of ^{28}Si (Ziegler et al., 2005a), mass-balance dictates that this cannot be maintained indefinitely, and at steady-state progression of weathering into a grain, the ^{30}Si/^{28}Si ratio of Si released must equal that of the grain (Geilert et al., 2015). The complete absence of river DSi of lower δ^{30}Si than bedrock also argues against this. We therefore consider that the range of δ^{30}Si in continental waters predominantly reflects fractionating processes occurring *after* solubilisation from the parent material.

Relatively large Si isotope fractionations are associated with secondary mineral formation, Si adsorption to Fe or Al oxides and biological uptake (summarised in Fig. 2). Note that because both abiotic and biotic processes are associated with similar fractionations, the two are isotopically comparable. For processes in the opposite direction – the dissolution of clay minerals or biogenic silica – the evidence for fractionation is more equivocal (Wetzel et al., 2014) for the reasons discussed above, and has been considered negligible in modelling of isotope behaviour in the weathering zone (Bouchez et al., 2013). Therefore to a first order δ^{30}Si of DSi in continental waters should be a function of i) the degree of net incorporation of solubilised Si into secondary

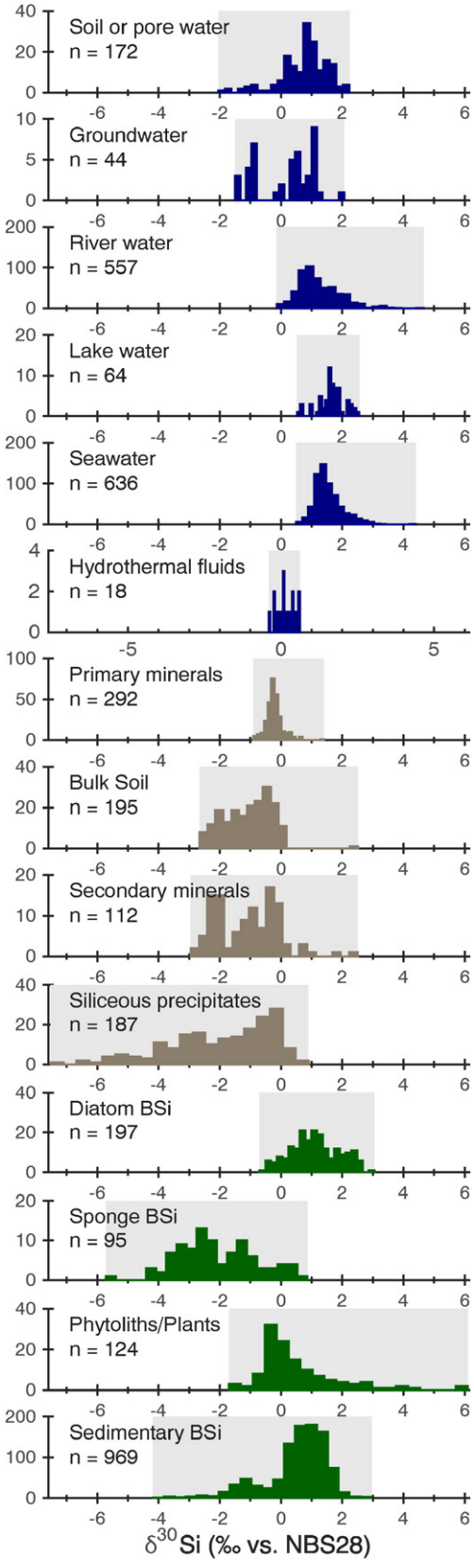

Fig. 4. A compilation of silicon isotope determinations on natural materials. The grey shaded area shows the range of values found in the literature, while the bars show the distribution of these values. Data sources: *Soil and pore waters*: Cornelis et al. (2010), Frings et al. (2014c), Pogge von Strandmann et al. (2012), Pokrovsky et al. (2013), White et al. (2012), Ziegler et al. (2005a,b), and Vandevenne et al. (2015). *Groundwater*: Douthitt (1982), Georg et al. (2009a,b), Opfergelt et al. (2011, 2013), Pokrovsky et al. (2013), Ziegler et al. (2005a,b), and Pogge von Strandmann et al. (2014). *River water*: Alleman et al. (2005), Cardinal et al. (2010), Cockerton et al. (2013), De la Rocha et al. (2000), Delvaux et al. (2013), Ding et al. (2004, 2011), Engström (2009), Engström et al. (2010), Fontorbe et al. (2013), Frings et al. (2014c, 2015), Frings (unpublished data), Georg et al. (2006, 2007a, 2009a), Hughes et al. (2011, 2012, 2013), Opfergelt et al. (2009, 2013), Pokrovsky et al. (2013), Ziegler et al. (2005a,b), and Vandevenne et al. (2015) *Lake water*: Alleman et al. (2005), Opfergelt et al. (2011), and Panizzo et al. (2016). *Seawater*: De La Rocha (unpublished compilation). *Hydrothermal fluids* (*including hot springs*): De La Rocha et al. (2000), Opfergelt et al. (2011, 2013), Douthitt (1982), Geilert et al. (2015), and Ding et al. (1996). *Primary minerals* (*non-exhaustive, includes metamorphic, igneous and sedimentary*): Abraham et al. (2008), Armytage et al. (2011), Basile-Doelsch et al. (2005), Chakrabarti and Jacobsen (2010), Cornelis et al. (2010), Douthitt (1982), Fitoussi and Bourdon (2012), Fitoussi et al. (2009), Frings et al. (2014c), Georg et al. (2007b, 2009b), Opfergelt et al. (2010, 2012), Pokrovsky et al. (2013), Savage et al. (2011, 2013), Steinhoefel et al. (2011), Zambardi et al. (2013), and Ziegler et al. (2005a,b). *Bulk soil*: Bern et al. (2010), Cornelis et al. (2010), Ding et al. (2005b), Opfergelt et al. (2010, 2012), Pogge von Strandmann et al. (2012), Pokrovsky et al. (2013), Steinhoefel et al. (2011), and Ziegler et al. (2005a). *Secondary minerals*: Cornelis et al. (2010, 2014), Ding et al. (1996), Douthitt (1982), Frings et al. (2014c), Georg et al. (2009b), Opfergelt et al. (2010, 2012), Steinhoefel et al. (2011), and Ziegler et al. (2005b). *Siliceous precipitates* (*silcretes, sinters and other precipitates*): Basile-Doelsch et al. (2005), Douthitt (1982), Geilert et al. (2015), and Ding et al. (1996). *Diatom BSi* (*marine and freshwater*): Alleman et al. (2005), Cardinal et al. (2007), De la Rocha et al. (2000), Fripiat et al. (2011), Opfergelt et al. (2011), Panizzo et al. (2016), Varela et al. (2004), and Sun et al. (2013). *Sponge BSi* (*mostly marine*): De La Rocha (2003), Douthitt (1982), Hendry and Robinson (2012), Hughes et al. (2013), and Wille et al. (2010). *Vascular plants/Phyotliths*: Cornelis et al. (2010), Ding et al. (2005b), Douthitt (1982), Engström et al. (2008), Frings et al. (2014c), Hodson et al. (2008), Köster et al. (2009), Opfergelt et al. (2010), Pokrovsky et al. (2013), Steinhoefel et al. (2011), White et al. (2012), and Ziegler et al. (2005b). *Sedimentary BSi*: Cockerton et al. (2015), Douthitt (1982), Frings et al. (2014c), Panizzo et al. (2016), Street-Perrott et al. (2008), Swann et al. (2010), and Sun et al. (2011), plus marine sediments as detailed in Fig. 8.

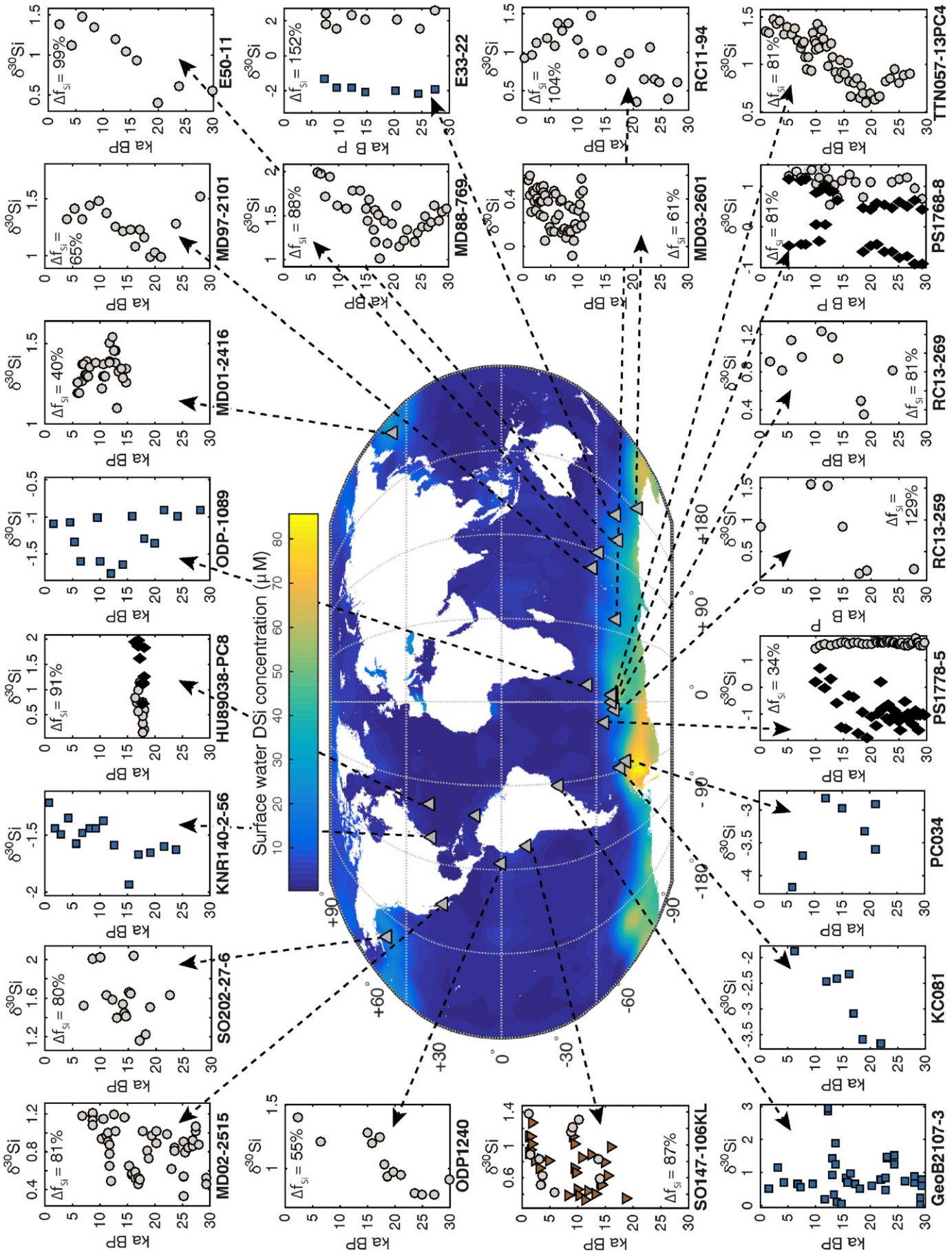
Surface water DSi concentration (µM)
10
20
30
40
50
60
70
80
+90°
+60°
+30°
0°
-30°
-60
-90°
-180°
0°
+90°
+180°
-90°
E50-11
Δf_Si = 99%
E33-22
Δf_Si = 152%
RC11-94
Δf_Si = 104%
TTN057-13PC4
Δf_Si = 81%
MD97-2101
Δf_Si = 65%
MD88-769
Δf_Si = 88%
MD03-2601
Δf_Si = 61%
PS1768-8
Δf_Si = 81%
MD01-2416
Δf_Si = 40%
ODP-1089
RC13-269
Δf_Si = 81%
HU89038-PC8
Δf_Si = 91%
RC13-259
Δf_Si = 129%
KNR140-2-56
PS1778-5
Δf_Si = 34%
SO202-27-6
Δf_Si = 80%
PC034
MD02-2515
Δf_Si = 81%
KC081
ODP1240
Δf_Si = 55%
SO147-106KL
Δf_Si = 87%
GeoB2107-3
δ30Si
ka BP

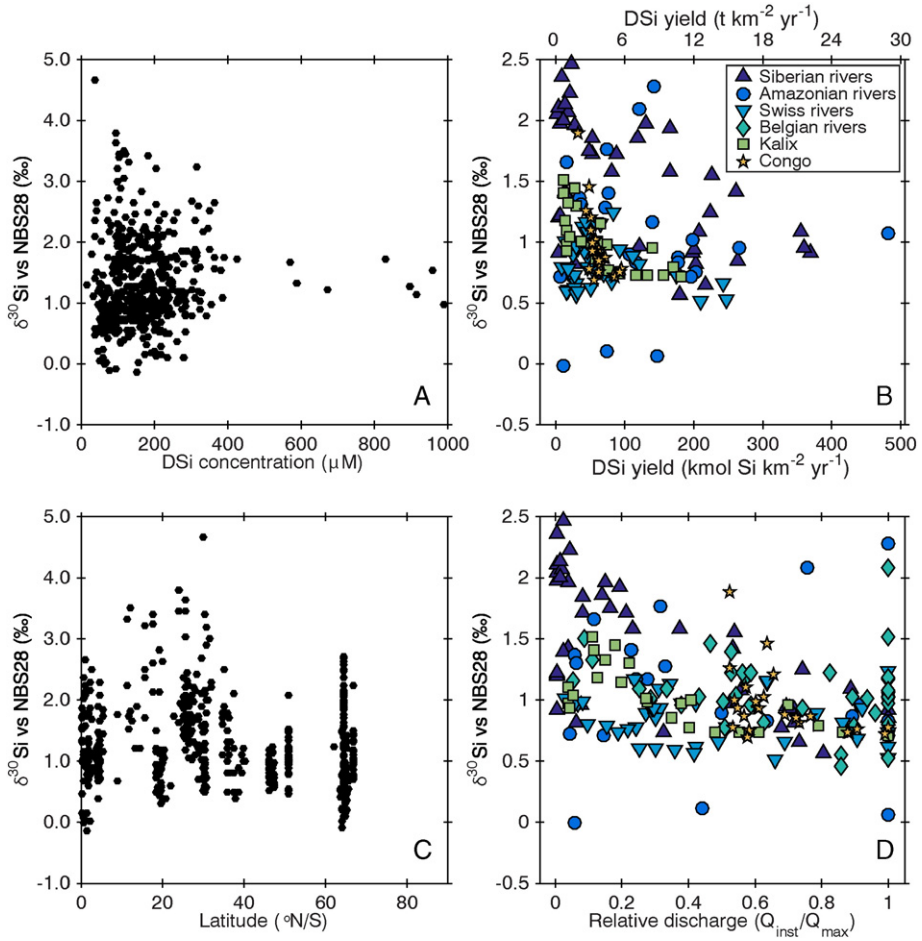

Fig. 6. Variation in δ^{30}Si of river DSi as a function of A: river DSi concentration (μM); B: instantaneous DSi yield (kmol km^{-2} yr^{-1}; the upper axis shows a conversion to t km^{-2} yr^{-1} for convenience); C: latitude (°N or S) and D: Instantaneous discharge (Q_{inst}) normalised to the maximum observed in a given river (Q_{max}).
Data sources as in Fig. 4.

minerals or biogenic silica and ii) the fractionation associated with this (Bouchez et al., 2013). This simple observation explains why all river waters and most soil- and ground-waters are ^{30}Si enriched relative to the DSi released from bedrock: the removal of DSi from solution to these neoformed solid phases preferentially incorporates the lighter ^{28}Si, with permil enrichments ($^{30}\varepsilon_{removal}$) that cluster around −1 to −2‰, though greater fractionations have been reported (Fig. 2).

3.1. Identifying incorporation of Si into secondary phases

Assuming that silicate minerals release Si and other elements stoichiometrically, and if one or more of these elements behaves conservatively in solution, then f_{Si}, the fraction of initially solubilised Si that remains in solution, can be estimated:

$$f_{Si} = {}^{DSi/X_{solution}} \Big/ {}_{Si/X_{parent}}$$

where $X_{solution}$ and X_{parent} are the concentrations of the normalising element(s) in the dissolved phase and the parent material, respectively. Hughes et al. (2013) used dissolved (Na + K) in the Amazon basin and Georg et al. (2007a) used dissolved Ca in Icelandic rivers. This index reflects weathering *congruency* — an f_{Si} of 1 implies that all Si initially mobilised remains in solution (*i.e.* solute element and isotope ratios identical to that of the parent material), whereas f_{Si} of 0 implies all Si has been removed from solution and incorporated into secondary solids, including biogenic silica. We follow Hughes et al. (2013) and use (Na + K) as normalising elements, with a parent upper crustal Si/(Na + K) molar ratio of 6.7 from Rudnick and Gao (2003), although a value of ~3.5 may be more appropriate, as it discounts the non-reactive quartz component (Hughes et al., 2013). Note that there are several caveats involved in the use of (Na + K) for normalisation, including the assumptions that there are no additional sources other than the silicate bedrock, and that they behave conservatively in solution, which are both commonly invalidated. Additionally, seasonal

Fig. 5. Variation in δ^{30}Si of biogenic silica in marine sediments over the last 30 ka. Data sources as in Fig. 7. Grey circles = diatoms; blue squares = siliceous sponge spicules; black diamonds = radiolarians; brown triangles = bulk biogenic silica. For measurements made on diatom BSi, the required change in utilisation efficiency (Δf_{Si}) is calculated for a case with constant initial δ^{30}Si of DSi, assuming a diatom fractionation of −1.1‰ and a steady-state isotope evolution model. Central map shows the location of marine sediment cores (red dots) referred to in this manuscript, previously studied for variation in δ^{30}Si of biogenic opal in the late Quaternary. Background is the world ocean surface water DSi concentration from Gouretski and Koltermann (2004). Data sources: *Core E50-11*: De La Rocha et al. (1998); *Core GeoB2107–3*: Hendry et al. (2012); *Core HU89038-PC8*: Hendry et al. (2014); *Core KC081*: Hendry et al. (2010); *Core KNR140-2-56GGC*: Hendry et al. (2010); *Core MD01-2416*: Maier et al. (2013); *Core MD01-2515*: Pichevin et al. (2012); *Core MD03-2601*: Panizzo et al. (2014); *Core MD88-769*: Beucher et al. (2007); *Core MD97-2101*: Beucher et al. (2007); *Core MD99-2198*: Griffiths et al. (2013); *Core ODP1240*: Pichevin et al. (2009); *Core ODP1089*: Ellwood et al. (2010); *Core PC034*: Hendry et al. (2010); *Cores PS1778-5 and PS1768-8*: Abelmann et al., 2015; *Core RC11-94*: De La Rocha et al. (1998); *Core RC13-259*: Brzezinski et al. (2002); *Core RC13-269*: De La Rocha et al. (1998); *Core SO147-106KL*: Ehlert et al. (2013); *Core SO202-27-6*: Maier et al. (2016); *Core TTN057-13PC4*: Horn et al. (2011); and *Core E33-22*: Ellwood et al. (2010) and Sutton (2011).

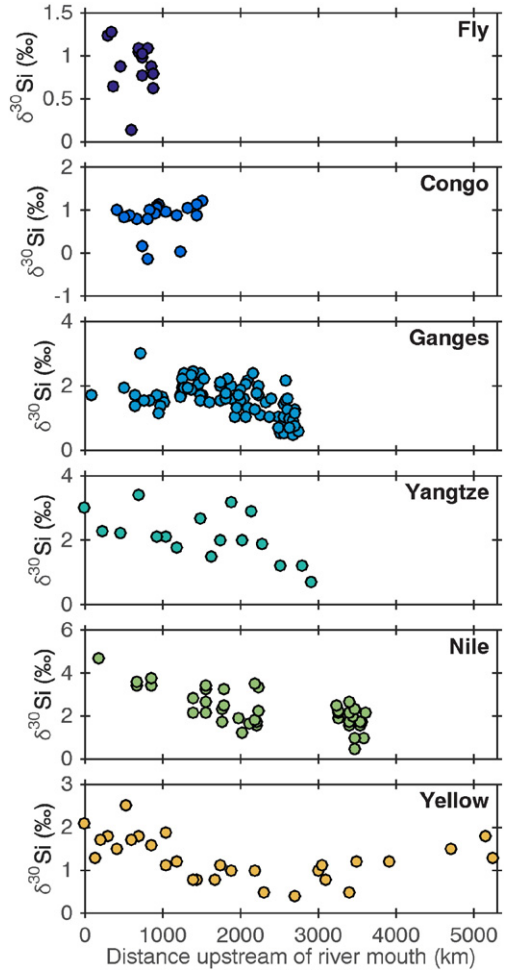

Fig. 7. Longitudinal change in river DSi δ^{30}Si. Fly: Frings (unpublished data); Congo: Cardinal et al. (2010); Ganges: Frings et al. (2015) and Fontorbe et al. (2013); Yangtze: Ding et al. (2011); Nile: Cockerton et al. (2013); Yellow: Ding et al. (2004).

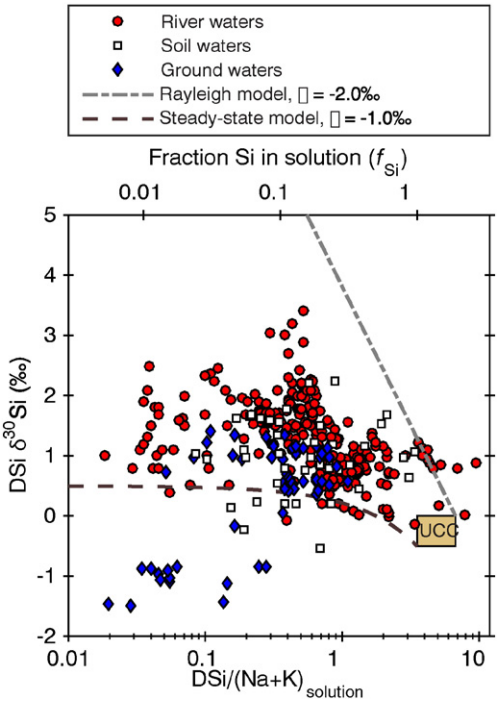

Fig. 8. Range of δ^{30}Si seen in DSi from rivers, porewaters and groundwaters as a function of DSi/(Na + K), a proxy for weathering congruency. The brown box shows an approximate endmember composition of the upper continental crust (UCC) (Rudnick and Gao, 2003; Savage et al., 2013), while the dashed lines show the expected evolution of δ^{30}Si expected as DSi is removed under two simple model scenarios: i) a finite-pool model which produces a Rayleigh distillation curve (*i.e.* a straight line in log-linear space) or ii) an open system (curved line in log-linear space), equivalent to the 'batch reactor' model of Bouchez et al. (2013). These two endmember models provide an envelope of permissible variability for any given system which will likely display behaviour intermediate between the two. The upper x-axis shows a conversion of DSi/(Na + K) to f_{Si}, the fraction of DSi remaining in solution, assuming a starting DSi/(Na + K) of 3.53 after Hughes et al. (2013).
Data sources as in Fig. 4, with additional geochemistry data from Bagard et al. (2011), White et al. (2009), Dowling et al. (2003) and Pogge von Strandmann et al. (2006, 2008) where necessary. Data were corrected for rainwater solute inputs only if available in the original publication.

biological activity can affect DSi concentrations (Conley, 1997; Fulweiler and Nixon, 2005), so the sampling needs to be time-averaged (or at least representative) — a condition rarely met. Finally, the use of a universal $Si/(Na + K)_{parent}$ for all rivers is questionable due to variability in primary mineral cation content.

Despite these caveats, it serves as a starting point for discussion. As plotted in Fig. 8, δ^{30}Si of continental water DSi trends towards higher values as it is progressively removed from solution (*i.e.* moving from right to left). Almost all river waters are accommodated within the envelope defined by the Rayleigh and steady-state fractionation models with molar $Si/(Na + K)_{parent}$ ratios of 3.5 or 6.7, and fractionations of −1‰ and −2‰, respectively. This normalisation procedure suggests that somewhere between 50% and >95% of the Si that is mobilised from parent material is reincorporated into secondary phases (upper x-axis), and that this is a first order control on the variability of silicon isotope ratios in river waters. But beyond this rather crude picture, many questions about the distribution of δ^{30}Si in continental waters remain. Why are soil and ground waters sometimes more negative than the parent material? What causes the large scatter in the evolution of δ^{30}Si as a function of f_{Si}?

In the following we briefly discuss three complicating factors: i) the potential for heterogeneous source material, ii) the potential for variable fractionation factors and iii) mass-balance constraints on the manifestation of isotopic fractionation.

3.1.1. Heterogeneous source material

The above discussion assumed that the parent material is relatively homogenous with regards to its silicon isotope composition. To explain the low (<0‰) values, it may be that the assumption of negligible variation in parent δ^{30}Si is invalid. This is the explanation favoured for low δ^{30}Si (−1.50–1.54‰) groundwater in Arizona (Georg et al., 2009b), the Ganges–Brahmaputra Delta (Georg et al., 2009a) and the Australian Great Artesian Basin (Pogge von Strandmann et al., 2014), where dissolution of (low δ^{30}Si) clay minerals is invoked as a source of low δ^{30}Si DSi.

3.1.2. Variable fractionation factors

Laboratory studies have demonstrated a reaction-rate and temperature dependency of silicon isotope fractionation, as well as a dependency on ambient dissolved Al concentrations (Geilert et al., 2014; Oelze et al., 2014, 2015; Roerdink et al., 2015). They have also demonstrated that instantaneous fractionations between solute and solid can be interpreted within the framework proposed by DePaolo (2011). This framework relates the net isotope fractionation to the ratio of forward and backward reaction rates (R_f and R_b respectively, representing mineral neoformation and (re)dissolution of the solid). These two reactions are associated with kinetic isotope fractionation factors (α_f and α_b), which are normally <1, so both favour the transfer of the light isotope.

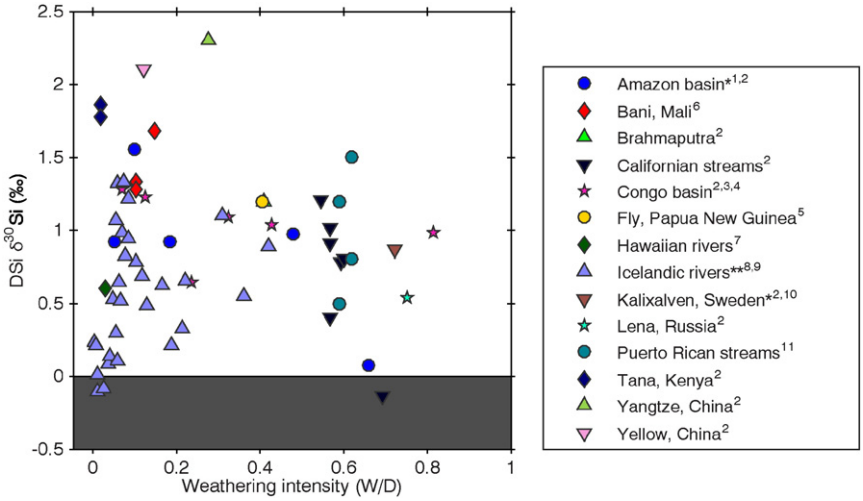

Fig. 9. Variation of δ^{30}Si of river DSi as a function of weathering intensity, as defined by Bouchez et al. (2014), where W refers to the rate of chemical weathering and D to the total (chemical plus physical) denudation rate. At both low and high weathering intensities, there is little silicon isotope fractionation since either close to 0% or close to 100% of Si is exported as solutes, respectively. The grey shaded region indicates the approximate isotopic composition of source material (*i.e. ca.* −0.25‰). *δ^{30}Si as weighted average of annually measured values; all other values are spot samples. **Chemical and physical erosion rates assumed to be captured by instantaneous total dissolved solids (TDS) and total suspended solid (TSS) data, respectively. *δ^{30}Si data sources*: *Amazon*: Hughes et al. (2013); *Brahmaputra*: Georg et al. (2009a) *Californian streams*: De La Rocha et al. (2000); *Congo basin*: Cardinal et al. (2010) and Hughes et al. (2011); *Fly River*: A. Kurtz (unpublished data); *Ganges basin*: Frings et al. (2015); *Hawaiian Rivers*: Ziegler et al. (2005a); *Icelandic rivers*: Opfergelt et al. (2013) and Georg et al. (2007a); *Kalixälven*: Engström et al. (2010); *Lena River*: Engström (2009); *Puerto Rican streams*: Ziegler et al. (2005b); *Tana River*: Hughes et al. (2012); *Yangtze*: Ding et al. (2004); *Yellow*: Ding et al. (2011). Superscripts refer to source of physical and/or chemical denudation rate data: 1: Gaillardet et al. (1997); 2: Milliman and Farnsworth (2011); 3: Dupré et al. (1996); 4: Laraque et al. (2009); 5: A. Kurtz (unpublished data); 6: Picouet et al. (2002); 7: Li (1988); 8: Vigier et al. (2006); 9: Opfergelt et al. (2013); 10: Land et al. (1999); 11: Riebe et al. (2003).

The net reaction rate, R_p is simply $R_f - R_b$, while the apparent fractionation factor, α_p is a function of the two fractionation factors and the ratio of the two reaction rates (see discussion in Oelze et al., 2014). At far-from-equilibrium conditions when $R_p \gg R_b$, the instantaneous $\alpha_p \approx \alpha_f$. Conversely, when R_p is small relative to R_b the reaction is at, or close to, isotopic equilibrium and α_p is equivalent to an equilibrium isotope fractionation factor, α_{eq}.

The magnitude of the equilibrium fractionation factor, α_{eq} between DSi and solid has been experimentally determined at −0.30‰ for Si adsorption onto Al-hydroxides (Oelze et al., 2014) and ~0‰ for amorphous silica precipitation (Roerdink et al., 2015). In the same experiments, the initial (kinetic) silicon isotope fractionations between solution and solid was determined at −1.8 to −3.0‰ (Oelze et al., 2014) and −0.7 to −3.5‰ (Roerdink et al., 2015), demonstrating that for any given process the associated fractionation cannot be assumed constant.

Interestingly, given the long formation times for secondary minerals, and the fact that many river waters are apparently at or close to chemical equilibrium (a prerequisite for isotopic equilibrium), then it might be expected that equilibrium isotope effects (with fractionations close to 0‰) should dominate (Dupuis et al., 2015). The consistently low δ^{30}Si of secondary minerals (Fig. 4) suggests this is not the case. Oelze et al. (2014) resolve this by proposing that the fractionation occurs during the initial Si absorption on Al-hydroxides, that are subsequently converted with no fractionation (no stoichiometric change) to more stable clay minerals *via* hydroxy-aluminosilicate intermediates. Alternatively, the surfaces of the neoformed solids may be at isotopic equilibrium with the surrounding fluids, while the bulk of the solid is protected.

3.1.3. The manifestation of isotopic fractionation

While the two isotope fractionation models in Fig. 6 adequately define the limits of allowable variation in δ^{30}Si of river DSi, no model provides a good fit to the global data. This may result from rivers inherently following either a Rayleigh or a steady-state isotope evolution, the explanation favoured by Hughes et al. (2013) for rivers of the Amazon basin and Georg et al. (2007a) for Icelandic streams. However, there is no reason to expect a given river – which integrates a suite of upstream processes – to correspond to one model. Strictly, the Rayleigh and steady-state models are applicable only to simple scenarios that may rarely be found in nature; the most likely case is an intermediate scenario.

Some rivers do seem to experience isotopic evolution approaching Rayleigh behaviour. The highest river δ^{30}Si values yet observed originate from rivers that flow though dry lowland regions, often with extensive irrigation systems (Cockerton et al., 2013; Ding et al., 2011). In these cases, evapotranspiration water losses can increase DSi concentrations, thereby a) reducing solubilisation of fresh DSi and b) promoting the precipitation and/or preservation of secondary phases, with associated kinetic isotope effects leaving the residual water ^{30}Si enriched. In other words, these systems approximate Rayleigh-type behaviour in that they are isolated from fresh inputs of DSi, while DSi is progressively removed.

Conversely, some rivers have very little isotopic fractionation between parent material and DSi, *i.e.* highly congruent weathering. As shown in Fig. 9, the lowest riverine δ^{30}Si values occur at either end of a weathering *intensity* spectrum, defined as the ratio of chemical erosion, W, to total denudation, D; where $D = W +$ physical erosion, E (Bouchez et al., 2014). At the high-intensity end (W/D near 1), these correspond to black-water rivers in tropical environments with soils that are almost completely desilicified (Cardinal et al., 2010; Hughes et al., 2013). At the low intensity end (W/D near 0), this corresponds to rivers that drain catchments with high physical erosion rates and low sediment residence times (Georg et al., 2006, 2007a). This implies the presence of a degree of equifinality to river δ^{30}Si which is a direct consequence of mass balance. In other words, there can be no observable fractionation if no secondary phases are formed (as in low intensity systems), or if all secondary phases are also re-solubilised (as in high intensity systems). In this way, we can see that a riverine δ^{30}Si value depends not just on the magnitude of the fractionation factor, but also whether the weathering regime permits it. This is broadly consistent with the steady-state isotope mass-balance model presented by Bouchez et al. (2013). This treats the weathering zone as a batch reactor in which the degree of isotopic fractionation observed in waters depends on the ratio of export of fractionated solid (*i.e.* clay or plant residue) to the production of solute from primary minerals.

Table 1
Summary of the modern day inputs of DSi to the global ocean, together with estimates of their Si isotope composition. Previous budgets (mass only) are shown for comparison. TDLR = Tréguer and De La Rocha (2013); T95 = Tréguer et al. (1995); WM83 = Wollast and Mackenzie (1983).

	This compilation					Previous budgets		
	DSi		δ^{30}Si			TDLR	T95	WM83
Flux	$\times 10^{12}$ mol yr^{-1}	±	‰	±‰ (1 sd)	Level of understanding	$\times 10^{12}$ mol yr^{-1}		
River DSi	6.33	0.36	1.25	0.68	OK	6.2 ± 1.8	5.6 ± 0.6	7.25
Estuarine removal	−0.63		+0.10		Poor	−1.5 ± 0.5	−0.6 ± *0.5*	
Dissolution of SPM	1.90	1.00	−0.18	0.25	Poor	1.1 ± 0.2	–	–
Groundwater DSi	0.65	0.54	0.19	0.86	Poor	0.6 ± 0.6	–	–
Dissolution of dust	0.30	0.20	−0.65	0.43	Poor	0.5 ± 0.5	0.5 ± 0.5	–
Hydrothermal fluids	0.60	0.40	−0.30	0.15	Poor	0.6 ± 0.4	0.2 ± 0.1	0.89
Low temperature alteration of oceanic crust	0.40	0.30	0.00	0.5	Poor	1.9 ± 0.7	0.4 ± 0.3	0.36
	9.55	1.31	0.74	0.17		9.4	6.1	8.5

For the majority of rivers that fall between these two weathering regime extremes, the manifestation of silicon isotope fractionation may be dependent on the kinetics of secondary phase formation. In other words, the longer fluids spend in the weathering zone, the longer secondary phases have to precipitate. At greater mean water residence times, clay mineral formation is increased, pushing δ^{30}Si higher. This interpretation is corroborated by δ^{30}Si changes along river longitudinal transects (Cardinal et al., 2010; Cockerton et al., 2013; Ding et al., 2004, 2011; Fontorbe et al., 2013; Hughes et al., 2012; Frings et al., 2015; Fig. 7). These studies show that there is a consistent tendency for δ^{30}Si to increase downstream, presumably as water and sediment residence times increase in the lowland portions of catchments. The greater interaction times implied should increase the degree of secondary mineral neoformation as the limits to clay precipitation (and therefore Si isotope fractionation) are overcome. A similar argument can be made based on the coincidence of the periods of lowest discharge (longest residence times) and highest δ^{30}Si values for annually monitored rivers (Delvaux et al., 2013; Engström et al., 2010; Georg et al., 2006; Hughes et al., 2011, 2013; Pokrovsky et al., 2013; Fig. 5d).

3.2. Outlook: understanding and interpreting δ^{30}Si of DSi in continental waters

Taken altogether, these observations pose problems for modelling and interpreting δ^{30}Si at the Earth surface because interpretation of δ^{30}Si values ultimately depends on an estimate of the fractionation between solution and solid. Yet the magnitude (and perhaps even the sign) of fractionation varies as a function of reaction rate, and the degree to which the fractionation is able to be manifest depends on the completeness of the reaction or transformation. This implies that Si dynamics within individual systems should be rigorously understood before interpretations are made based on silicon isotope ratios. Note also that removal of DSi to biotic (diatoms, vascular plants) or abiotic (clays, Fe-oxides) phases cannot be inferred based on δ^{30}Si of the residual DSi alone.

4. Present-day inputs of DSi to the global ocean

The most important sources of DSi to the global ocean are supplied by the continental fluvial system. Chiefly, these are (i) DSi in rivers and (ii) groundwaters, and (iii) the dissolution of river particulate matter. DSi deriving from these sources must first pass through many fluvial 'filters', including wetlands, lakes, floodplains, estuaries and the coastal zone before reaching the open ocean. Other inputs include (i) the dissolution of aeolian dust and (ii) seafloor weathering and hydrothermal fluid circulation. In this section, the state-of-the-art regarding knowledge of the magnitude and isotopic compositions of the inputs to the ocean are presented (summarised in Table 1). We explore the derivation of each term in the budget and highlight associated uncertainties and knowledge gaps.

4.1. River DSi flux

4.1.1. Magnitude of river DSi flux

The modern river DSi flux is reasonably well constrained. DSi is easily measurable and has limited speciation over the pH range of meteoric waters (Iler, 1979). Global estimates of river DSi fluxes span almost a century (Beusen et al., 2009; Clarke, 1924; Dürr et al., 2011b; Livingstone, 1963) and are surprisingly consistent despite differences in data availability and upscaling procedures. Average river water DSi concentrations are *ca.* 160 μM (9.5 mg l^{-1} SiO_2) (Dürr et al., 2011b). A nutrient export model using a stepwise multiple linear regression approach and developed at the watershed scale (NEWS-DSi) (Beusen et al., 2009) predicts DSi fluxes of 6.33×10^{12} mol yr^{-1} to the coastal ocean, with 2.5–97.5 percentile values at 5.66 and 7.11×10^{12} mol yr^{-1}, respectively. A similar approach (Dürr et al., 2011b) uses essentially the same data but extrapolates at the scale of pre-defined coastal segments to arrive at a similar estimate (6.18×10^{12} mol yr^{-1}), lending further confidence to the NEWS-DSi model, whose output we retain as the best estimate of river DSi fluxes.

4.1.2. δ^{30}Si of river DSi flux

To date, at least 557 δ^{30}Si determinations exist for river water DSi (Fig. 4). These span from −0.14‰ to 4.66‰ with a mean of 1.28‰ (n = 544) and follow a roughly normal distribution (Fig. 4) with a standard deviation of 0.68‰. It is worth noting that seasonal and longitudinal variability in river DSi δ^{30}Si is typically large, on the order of 1.0‰. As noted above δ^{30}Si generally (i) decreases with increasing discharge and (ii) increases with distance downstream. In the absence of many rivers sampled over an annual period near their mouths, we retain the simple mean of 1.28 ± 0.68‰.

4.1.3. The role of estuaries in modulating river Si fluxes

The estimates of sediment and DSi delivery *via* rivers to the ocean are based on sampling of the river freshwater endmember, often a considerable distance upstream of its entrance to the ocean. It is acknowledged that storage of sediment fluxes between gauging stations and the end of the freshwater endmember may perhaps cause global sediment delivery to be overestimated (Allison et al., 1998; Milliman and Farnsworth, 2011). A similar problem exists with DSi as the river passes through the salinity gradient and across a continental shelf to reach the open ocean. Estuarine and other coastal environments are often highly productive, owing to their proximity to continentally sourced nutrients. If this production removes Si and permanently stores it in estuarine or deltaic sediments, then the amount of DSi entering the global ocean will correspondingly decrease. Removal of DSi will be manifest

as non-conservative mixing between the freshwater and saline endmembers (Bien et al., 1958), and can occur biologically (Conley and Malone, 1992) and abiotically (Chou and Wollast, 2006). Diatom blooms in the mixing zone may consume up to 50% of riverine DSi in the Amazon River (DeMaster, 2002) and almost 100% in the Scheldt (Chou and Wollast, 2006), although most of this will be regenerated. Using published transects along salinity gradients, DeMaster (2002) inferred 0.6×10^{12} mol Si yr^{-1} for estuarine Si removal based on the degree of non-conservative mixing, which we use in our budget (Table 1). The global estuarine surface area is ~1.1×10^6 km^2 (Dürr et al., 2011a), implying a sedimentation rate of ~33 g SiO_2 km^{-2} yr^{-1}, close to lake sedimentation rates (Frings et al., 2014a), and lower than the few estuarine BSi accumulation rates found in the literature (60–500 g SiO_2 km^{-2} yr^{-1}) (Colman and Bratton, 2003; Qin et al., 2012; Carbonnel et al., 2013).

Previous ocean Si budgets have included reverse weathering in estuarine or deltaic regions as a discrete loss term (Tréguer et al., 1995; Tréguer and De La Rocha, 2013). The term reverse weathering refers to the formation of authigenic clay minerals in continental margins, and was first proposed to balance ocean element budgets (Mackenzie and Garrels, 1966) — indeed, it is known to be a key sink for many elements. Reverse weathering is thought to occur as a result of the interaction of degraded continental aluminosilicates with ocean porewaters following the approximate reaction scheme: (alumino)silicate + cations + SiO_2 + HCO_3^- = cation-rich aluminosilicate + CO_2 + H_2O. This process occurs in different settings, and has been inferred indirectly from porewater profiles (Mackenzie and Kump, 1995; März et al., 2015; Michalopoulos and Aller, 1995, 2004), observed in situ (Michalopoulos et al., 2000; Presti and Michalopoulos, 2008), or experimentally replicated (Loucaides et al., 2010). It is suggested to account for up to 25% of DSi removed from the ocean (Holland, 2005). However, porewaters of marine sediments are almost exclusively enriched in DSi relative to the overlying water column (März et al., 2015; Ragueneau et al., 2000); the benthic DSi flux across the sediment/water interface is always positive. In this context, reverse weathering should be considered as a diagenetic pathway for BSi (Aller, 2014) that enhances its preservation efficiency, rather than being a sink *per se*.

4.1.4. Isotopic effect of estuarine Si removal

DeMaster (2002) estimated that ~10% of river DSi is sequestered within estuaries today as biogenic silica. If this is associated with a typical fractionation of −1.1‰ (De La Rocha et al., 1997), then the $\delta^{30}Si$ of river DSi entering the ocean is shifted towards a higher value by ~0.11‰ due to the presence of an estuarine filter, assuming no fractionation associated with reverse weathering. There is little work available to test this conclusion, and the available studies are equivocal. In the Tana River, Kenya, DSi mixes conservatively along the salinity gradient so there is no Si isotope fractionation (Hughes et al., 2012). In the Lena River delta, DSi is removed along the salinity gradient, but counter to expectations $\delta^{30}Si$ also decreases (Engström, 2009), interpreted as mixing with an unidentified ^{30}Si deplete water mass. Conversely, in the Elbe River estuary (Weiss et al., 2015) and the tidal freshwater section of the Scheldt river (Delvaux et al., 2013), DSi concentrations are depleted – presumably by biological activity – and $\delta^{30}Si$ of the residual DSi increases as expected, at least during the times of the year in which silicifying organisms grow.

4.2. Dissolution of river particulate matter

4.2.1. Magnitude of DSi flux from dissolution of river particulate matter

River suspended particulate matter (SPM) is predominantly silicate material (Viers et al., 2009), some of which will dissolve in the ocean. Conventionally, river SPM is assumed to dissolve sufficiently slowly that it does not contribute to biological cycling. However, it need be only sparingly reactive to have a large effect (Oelkers et al., 2011; Jeandel and Oelkers, 2015), and recent work suggests that dissolution, desorption or ion-exchange of river SPM in estuaries and the coastal zone is indeed large enough to be a substantial component of ocean elemental or isotope budgets (Gislason et al., 2006; Jeandel et al., 2011; \ et al., 2014; Oelkers et al., 2011). Estimates of the magnitude of the total river particulate flux cluster around 14–20 × 10^9 t yr^{-1} (*e.g.* Milliman and Meade, 1983; Syvitski et al., 2005) with a recent estimate being 19 × 10^9 t yr^{-1} (Milliman and Farnsworth, 2011). How much of this SPM will dissolve in the ocean? Insight can be gained by considering the amount of BSi carried by rivers, or by simple experimental approaches exploring the interaction of river sediment and seawater.

4.2.1.1. River transport of biogenic silica. Conley (1997) quantified the BSi material carried by rivers at $1.05 \pm 0.20 \times 10^{12}$ mol yr^{-1}, based on a simple extrapolation of surface water samples from a small dataset of 11 rivers. However, with a growing awareness that the conventional measurement protocols (weak alkali leaches, *e.g.* DeMaster, 1981) do not target BSi *per se*, but rather a range of non-crystalline siliceous phases, the term 'amorphous silica' (ASi) is now more prevalent (Barão et al., 2014, 2015), although some fraction of river SPM can indeed be 'true' BSi (Cary et al., 2005; Meunier et al., 2011). Dissolution rates of ASi are greater, by around a factor of 5, in the higher pH and electrolyte concentrations of seawater relative to freshwater (Loucaides et al., 2008, 2012). As a result, the ASi fraction is assumed to dissolve rapidly along the salinity gradient, an assumption generally borne out in studies of estuarine particulate matter (Carbonnel et al., 2013; Lehtimäki et al., 2013; Pastuszak et al., 2008). Frings et al. (2014b) showed that in the Ganges basin, the Si extracted by a conventional weak alkali leaching protocol (DeMaster, 1981) is a relatively consistent fraction (mean ± σ = 1.2 ± 0.78%) of the total sediment load. Extending the calibration dataset to include 415 paired and globally distributed ASi-SPM measurements, Frings (2014) estimated that ~0.6% of global river SPM is 'ASi'. Taking a total SPM flux of 19 × 10^9 t, this implies that 1.9×10^{12} mol yr^{-1} ASi is carried by rivers.

4.2.1.2. Experimental approaches. Experimental work to investigate the interaction of river sediment and seawater has mostly used riverbed material from basaltic islands (e.g. Jones et al., 2012a,b; Pearce et al., 2013; Oelkers et al., 2011), though Jones et al. (2012b) also used material from the Amazon, Mississippi and Orange rivers. Over the full course of these experiments, only about 0.005 to 0.01% of the Si in the sediment was solubilised. However, given the high solid:solution ratios (*ca.* 1:3), a near-equilibrium concentration was quickly obtained (≪1 month), impeding further dissolution. Focusing on basaltic glass, Morin et al. (2015) confirmed Si dissolution rates increase as a function of salinity. Their experiments were conducted at 90 °C, and based on an extrapolation to 16 °C and assumptions about the quantity of sediment deriving from volcanic islands, they argue 2–8 × 10^{12} mol Si yr^{-1} is released from basaltic glass dissolution alone, broadly equivalent to the river DSi flux. The young, basaltic sediment used in these studies is known to have high dissolution rates (Dupré et al., 2003) but is unlikely to be representative of global river SPM. These problems hamper extrapolation of the results to a global scale — further field or lab-based approaches in granitic or meta-sedimentary terrains are required. Nevertheless, they demonstrate the potential importance of dissolution of terrigenous material, which is reinforced by a mass-balance of the Mediterranean Si cycle that invokes dissolution of 1% of river SPM to close the budget (Jeandel and Oelkers, 2015).

Given that the ASi content of river SPM is of a very similar order of magnitude (see above), this suggests the two approaches at least partially target the same Si. The relevant questions then become: (i) To what extent do the measurement protocols for river ASi reflect the behaviour of river sediment in seawater? (ii) To what extent do the extraction protocols target amorphous silica? and (iii) To what extent is there a discrete ASi pool? These questions require further research. For the time being, we assume that the protocols developed for BSi

analysis (*e.g.* DeMaster, 1981) fortuitously capture the amount of all Si likely to dissolve in seawater – both amorphous and lithogenic – and therefore take a flux of 1.9×10^{12} mol yr^{-1} as the input of DSi to the ocean from terrigenous sediment dissolution, which may need revising upwards if the results of Morin et al. (2015) can be confirmed.

4.2.2. δ^{30}Si of DSi flux from dissolution of river particulate matter

The δ^{30}Si of bulk SPM has been measured only in the Yellow and the Yangtze rivers (Ding et al., 2004, 2011). Both systems have low δ^{30}Si SPM (mean $\pm$ 1 σ = -0.02 ± 0.20‰ and -0.34 ± 0.19‰, respectively). The δ^{30}Si of ASi has never been directly assessed in river sediment, although we can extrapolate from terrestrial ecosystem studies that these phases, whether formed biogenically (*e.g.* diatoms, phytoliths) or inorganically (*e.g.* poorly crystalline aluminosilicates), should tend towards even lower δ^{30}Si (Fig. 4). For now, we take the mean of the Yellow and Yangtze rivers of -0.18 ± 0.25‰ as representing the Si isotopic composition of terrigenous sediment.

4.3. Submarine groundwater discharge (SGD)

4.3.1. Magnitude of DSi flux from submarine groundwater discharge

It has long been recognised that the discharge of water from groundwater directly into the ocean may be a significant term ecologically, chemically and volumetrically (Johannes, 1980). Even if the flow rates are low, integrated over the entire length of a shoreline and combined with the generally higher solute concentrations in groundwater, SGD fluxes can be important (Moore, 1996). There is some confusion regarding the definition of submarine groundwater discharge. It is generally taken to mean any flow of water out across the seafloor, and so includes both the terrestrially derived freshwater endmember and a much larger recycled seawater component (Burnett et al., 2006). Here, we restrict ourselves to the component that derives directly from terrestrial infiltration of meteoric waters, although if the recirculating component interacts substantially with continental silicates it could be an important and completely unexplored term in the global Si cycle. The patchy and variable nature of this water flux has made it difficult to quantify (Burnett et al., 2006). Nevertheless, significant regional inputs of DSi from SGD have been demonstrated in *e.g.* the Mediterranean (Rodellas et al., 2015; Weinstein et al., 2011), the Bay of Bengal (Georg et al., 2009a) and from volcanic islands (Schopka and Derry, 2012).

To our knowledge, the only global estimates of the SGD contribution to the ocean Si budget are 0.4 and 0.6×10^{12} mol DSi yr^{-1} to the oceans, or approximately 6–10% of the river DSi flux (Laruelle et al., 2009; Tréguer and De La Rocha, 2013). These are based on the product of a total SGD of 2000 km^3 yr^{-1} (adapted from Slomp and Van Cappellen, 2004) and an arbitrarily assigned groundwater DSi concentration of 200 or 340 μM. Building on this approach, we note that estimates of the volume of SGD (Slomp and Van Cappellen, 2004; Knee and Paytan, 2011; Burnett et al., 2006; Taniguchi et al., 2002) range from 0.1 to 10% of the global river flux (which is approximately 37×10^3 km^3 yr^{-1}; Dai and Trenberth, 2002). These estimates are commonly based on global water budgets, with SGD being the residual of the other terms, such that the propagated uncertainty is of the same order of magnitude as the flux itself. Nonetheless, a consensus seems to be developing for a total flux of approximately 5% of river discharge, *i.e.* 1850 km^3 yr^{-1}, which we retain as the total SGD water flux with an uncertainty of $\pm$50%.

We now turn our attention to the 'mean' groundwater DSi concentration. To our knowledge, no systematic survey of global groundwater geochemistry is available. A geochemical survey of 1785 European bottled waters yields a mean $\pm$ 1σ DSi concentration of 319 $\pm$ 285 μM (Birke et al., 2010). Querying the database maintained by the USGS (the 'National Water Information System'/'Water Quality Samples for the Nation') for all well data in the USA, for measurements made in 2014, yields mean $\pm$ 1σ DSi concentration of 380 $\pm$ 250 μM (n = 2081). Based on 2640 datapoints from regional datasets, mostly from the continental United States, Davis (1964) suggested a median concentration for groundwater DSi of 300 μM. We take the mean of the USGS data of 380 $\pm$ 250 μM as representing the concentration of DSi in groundwater inputs to the ocean. Combining this with the total volume of SGD flow, we obtain a total SGD DSi flux of 0.65 $\pm$ 0.54×10^{12} mol yr^{-1}, or about 10% of the river DSi flux.

4.3.2. δ^{30}Si of DSi flux from submarine groundwater discharge

The range of δ^{30}Si reported for groundwater DSi is large (Fig. 4) and spans from -0.15‰ to $+1.34$‰ at various depths in the Bengal Basin (Georg et al., 2009a), from $+0.35$‰ to $+1.01$‰ for Icelandic springs (Opfergelt et al., 2011), from -1.42 to $+0.56$‰ along a 100 km flowpath in a sandstone aquifer in Arizona (Georg et al., 2009b) and from -1.50 to -0.85‰ in the Great Artesian Basin, Australia (Pogge von Strandmann et al., 2014). Isolated values of $+0.3$‰, $+0.5$‰ and $+0.7$‰ have also been reported in Hawaiian systems (Ziegler et al., 2005a,b), and up to $+2.07$‰ in a Siberian permafrost landscape (Pokrovsky et al., 2013). Unsurprisingly, given the diversity of systems and processes, there is no relationship between groundwater DSi concentration and δ^{30}Si. We therefore take the mean of the 44 published values (Fig. 4) of $+0.19$‰, with a range of 0.9‰, as representing the δ^{30}Si of groundwater DSi inputs to the ocean.

4.4. DSi inputs from dissolution of atmospheric dust

4.4.1. Magnitude of DSi flux from dissolution of aeolian dust

Existing estimates of DSi inputs from aeolian dust are essentially back-of-the-envelope calculations based on deposition rates and estimates of the fraction liable to dissolve as a function of residence time in the water column. All global Si budgets to date (Laruelle et al., 2009; Tréguer et al., 1995; Tréguer and De La Rocha, 2013) take a value of 0.5×10^{12} mol Si yr^{-1}. How realistic is this value?

Somewhere between 500 and 5000×10^{12} g dust yr^{-1} is currently entrained into the atmosphere (Engelstaedter et al., 2006), of which 134 to 910×10^{12} g yr^{-1} is deposited in the oceans (Duce et al., 1991; Jickells et al., 2005). This is mostly in the form of wet deposition, *i.e.* scavenged by precipitation, although gravitational ('dry') settling of larger particles may be important in nearshore environments (Prospero and Arimoto, 2008). If the composition of the upper continental crust (Rudnick and Gao, 2003) reflects the composition of mineral dust, some 67% is SiO_2. In other words, somewhere between 1.5 and 10.2×10^{12} mol Si yr^{-1} is deposited on the ocean surface.

Anywhere between <1% to more than 10% may potentially dissolve (Guerzoni et al., 1999; Tegen and Kohfeld, 2006), and a single value is hard to prescribe given regional differences in source composition, particle size, etc. Ridgwell et al. (2002) take a solubility of 6.6% for their model study, and Maring and Duce (1987) estimated up to 8–10% of Al contained in aerosol aluminosilicates would dissolve in seawater within 60 h. Using values of 1.5% to 5% for the fraction of dust which dissolves reasonably reproduce the distribution of global surface-ocean dissolved Al (Gehlen et al., 2003; Han et al., 2008; Measures and Vink, 2000). Si and Al co-occur as aluminosilicates, so assuming the same solubility for Si as Al (*i.e.* 1.5 to 5%, while acknowledging they have different fates in solution), provides DSi inputs from aerosol dissolution of 0.023 to 0.50×10^{12} mol Si yr^{-1}, so the Tréguer and De La Rocha (2013) estimate (0.5×10^{12} mol yr^{-1}) is probably an upper bound. Clearly, the two key terms in this derivation (dust deposition rates and Si solubility) need much better quantification.

4.4.2. δ^{30}Si of DSi flux from dissolution of aeolian dust

In the absence of direct measurements, there are two means of identifying the silicon isotope composition of aeolian dust. The mean of published bulk soil δ^{30}Si determinations (Fig. 4), equal to -1.08 ± 0.77‰ (n = 195), may suffice if soils can be considered broadly representative of the sources of dust to the ocean. Alternatively, the Pleistocene loess samples analysed by Savage et al. (2013) provide a mean of $-0.22 \pm$

0.07‰ (n = 13), and a similar value of −0.2‰ provided plausible results in an endmember analysis of Si sources in the glacial East Philippines Sea (Xiong et al., 2015). However, loess deposits tend to be towards the larger end of the dust size spectrum (Muhs, 2013), while the long-range transport particles that enter the marine realm may be smaller clays that tend towards lower δ^{30}Si values. We therefore take a value intermediate between soils and loess of −0.65‰, but suggest that it should be empirically determined in future.

4.5. Non-continental sources of DSi

Interaction between seawater and ocean basalts is an important control on seawater chemistry on geological timescales (Staudigel, 2014). Seawater flows through the permeable upper oceanic crust, where it may be heated by residual heat. Alkalinity, cations and DSi can derive from the reactions that occur. Compiling the available literature, Tréguer and De La Rocha (2013) estimate that the high temperature, axial component of fluid recirculation introduces 0.2–0.8 × 10^{12} mol Si yr^{-1}, and the low temperature ridge component 0–0.15 × 10^{12} mol Si yr^{-1}. We retain this estimate, in total *ca.* 0.6 ± 0.4 × 10^{12} mol DSi yr^{-1} from hydrothermal systems. This DSi probably has an initial δ^{30}Si value of −0.4 to −0.2‰, based on two samples collected at the East Pacific Rise by the submersible Alvin at ~300 °C and 11–15 mM DSi (De La Rocha et al., 2000), but this may change as the expelled fluid cools and becomes supersaturated, inducing silica precipitation. Whether or not precipitation of silica in such a process is important and if it is associated with isotope fractionation is unclear. The siliceous sinter deposits associated with hydrothermal or hot spring systems tend to be ^{30}Si depleted (Douthitt, 1982; Ding et al., 1996), implying the presence of an associated fractionation, perhaps as large as −4.4‰ (Geilert et al., 2015) although the effect on the residual DSi will depend on the proportion of the fluid DSi that is precipitated.

DSi can also be supplied from weathering of seafloor basalt, although the distinction between solutes deriving from hydrothermal fluid circulation and basalt weathering is ultimately arbitrary. Tréguer et al. (1995) included low-temperature alteration in their budget at 0.4 ± 0.3 × 10^{12} mol yr^{-1}, which can be traced to Maynard (1976) and Wolery and Sleep (1976) who invoked basalt alteration to balance ocean elemental budgets. Based on benthic DSi efflux rates, Tréguer and De La Rocha (2013) updated this value to 1.9 × 10^{12} mol DSi yr^{-1}, but including dissolution of terrestrial lithogenic material which we separated above. We therefore retain the earlier Tréguer et al. (1995) estimate of 0.4 ± 0.3 × 10^{12} mol yr^{-1}. Its δ^{30}Si value is also uncertain: secondary aluminosilicates are common in altered seafloor basalts, confirming that alteration is incongruent and therefore probably associated with Si isotope fractionation. We provisionally take 0.0 ± 0.5‰, but note that high and low-temperature hydrothermal fluids are probably isotopically distinct. It should be highlighted that DSi fluxes deriving from oceanic basalt are perhaps the most poorly understood and unconstrained in the global Si cycle.

4.6. Synthesis of DSi inputs to the global ocean

Based on the above, a total annual input of DSi to the modern ocean can be calculated at 9.55 ± 1.30 × 10^{12} mol with a flux-weighted δ^{30}Si of 0.74 ± 0.17‰ (Table 1). To our knowledge, this is the first estimate of the ocean δ^{30}Si budget. Note that of the component fluxes, few are known to a reasonable degree of precision. Uncertainties are hard to prescribe given the limited data availability. The total ocean volume is ~1.3 × 10^{21} l. According to the gridded climatology of Gouretski and Koltermann (2004), there is an average DSi concentration of 88 μmol kg^{-1} (or *ca.* 85 μmol/l^{-1}), for a total mass 112 × 10^{15} mol. For total inputs of 9.55 × 10^{12} mol yr^{-1} the estimated residence time for dissolved Si in the global ocean, defined as inventory/input, is just under 12,000 years. This is towards the lower end of previous estimates that cluster around 15,000 to 20,000 years (Broecker and Peng, 1982; Laruelle et al., 2009; Quinby-Hunt and Turehian, 1983; Sarmiento and Gruber, 2006; Tréguer et al., 1995). These typically have a similar total inventory of DSi; the smaller residence time derived here is a result of more inputs being considered and is consistent with that calculated by Tréguer and De La Rocha (2013) (~10,000 years).

5. Potential for variability in continent-ocean Si fluxes

If we understand the parameters that control the magnitude and isotopic composition of the Si fluxes to the ocean, we can use this understanding to place limits on how much Si fluxes to the ocean may vary. Given the *ca.* 12 ka residence time of Si in the ocean (Section 5), perturbations to the inputs must occur on similar timescales to affect ocean Si cycling (Richter and Turekian, 1993), so we focus on the processes that affect continental Si cycling over these timescales.

The world at the Last Glacial Maximum (LGM, *ca.* 21 ka BP) differed greatly to the modern world. Climate was generally cooler and drier and large ice sheets existed at high latitudes in both hemispheres. As a consequence, sea level was lower, newly exposing land surfaces and the distribution of terrestrial vegetation was drastically altered. In the following, we evaluate how each of these four main changes (climate, ice sheet extent, sea-level and vegetation zonation) may have altered the magnitude and isotopic composition of land-to-ocean Si fluxes. The aim of this exercise is to define plausible ranges that land-to-ocean Si fluxes may have varied within. These ranges can then be used to create scenarios of change in global land-to-ocean Si fluxes that act as inputs to a simple model to evaluate the timescales and magnitudes of whole-ocean δ^{30}Si response to a variable continental Si cycle.

5.1. Impact of glacial climate on land-to-ocean Si fluxes

5.1.1. Impact of glacial climate on the river DSi flux and δ^{30}Si

The river DSi flux is the single largest input to the ocean, but inferring potential variability on glacial–interglacial (G–IG) timescales is difficult, partly because the parameters controlling DSi fluxes are not well understood and are probably compensatory to some degree (Kump and Alley, 1994). The flux, and its associated δ^{30}Si, can vary in two ways:

1. *Via* changes in the rate of DSi release from primary minerals (*i.e.* the silicate weathering rate) and the weathering style, including changes associated with the exposure of continental shelf during sea-level lowstands and subglacial weathering.
2. *Via* changes in continental Si cycling, particularly the presence and efficiency of continental Si sinks (Billen et al., 1991; Meybeck and Vörösmarty, 2005).

What controls DSi mobilisation from bedrock? First-order controls on silicate-weathering rates include temperature, water availability and lithology, plus the tectonic parameters that affect the exposure of new material (West et al., 2005). These parameters control *e.g.* the degree of soil development, physical erosion rates, catchment hydrology and ecosystem structure which may be more direct determinants of silicate weathering rates. In practise, this makes it hard to predict how silicate-weathering rates may have varied over G–IG cycles. As Kump and Alley (1994) note, intuition is of little help because of the multiple interacting and counteracting controls.

We consider that the river DSi flux has been relatively invariant (±20%) since the LGM. This premise is based on modelling of river DSi fluxes using lithology-specific runoff–Si flux relationships (Jones et al., 2002; Gibbs and Kump, 1994; Munhoven, 2002). This work has demonstrated that a decrease in Si fluxes resulting from *e.g.* lower continental precipitation was largely balanced by increased fluxes from newly-exposed continental shelf. It is also consistent with interpretations of G–IG records of Pb stable isotopes in oceanic ferromanganese crusts (Foster and Vance, 2006), high-precision radiogenic ^{87}Sr/^{86}Sr ratios in foraminifera (Mokadem et al., 2015) and cosmogenic ^{10}Be/^{9}Be

ratios in ocean authigenic sediments and ferromanganese crusts (von Blanckenburg et al., 2015). These independent lines of evidence all suggest that the continental weathering fluxes have not substantially varied over the late Quaternary glacial–interglacial cycles; we make the simplifying assumption that the same is true for DSi fluxes.

However, the δ^{30}Si of the river DSi flux might be more variable. River DSi δ^{30}Si primarily reflects weathering congruency (Section 3, Fig. 6), so if this could be inferred or reconstructed it can constrain the magnitude of any change in river δ^{30}Si. Qualitatively, we suggest that the river DSi at the LGM likely had a lower associated δ^{30}Si. Dosseto et al. (2015) present an increase in lithium isotope ratios of 7‰ in clays in Himalayan fluvial terraces since the LGM, attributed to a corresponding decrease in weathering congruency. This is relevant because mass-balance dictates that the residual solutes should follow a similar trend (*cf.* Fig. 2), and the Si and Li isotope systems are thought to behave similarly (Opfergelt et al., 2013; Pogge von Strandmann et al., 2012), so glacial river DSi should also have lower δ^{30}Si. Note that no similar studies exist for silicon isotopes: there is clear potential for the δ^{30}Si of secondary minerals in *e.g.* fluvial terraces, floodplain deposits or deltaic sediments to provide useful insight into palaeo-weathering dynamics. Mechanistically, lower glacial river δ^{30}Si may result from (i) reduced catchment fluid and/or sediment residence times, (ii) lower temperatures acting to lower rates of secondary mineral formation *via* a reduction in the rate constants of precipitation or (iii) the greater relative formation of 2:1 clays over 1:1 clays, which tends to be associated with a smaller magnitude of fractionation (Opfergelt et al., 2012). Altogether, these can act to reduce the total magnitude of clay formation (increase weathering congruency), and therefore reduce the expression of Si isotope fractionation during glacials. We suggest a conservative reduction of 0.2 ± 0.25‰ of river DSi at the LGM relative to today.

5.1.2. Impact of glacial climate on the dust flux and δ^{30}Si

Marine and terrestrial sediments and ice-cores from both poles consistently show increased dust accumulation rates over the LGM (Muhs, 2013). Glacial dust fluxes have received attention for their potentially important role as a source of nutrients (particularly Fe or Si) to regions of the oceans where (siliceous) primary production is currently limited by lack of these nutrients (Harrison, 2000; Jickells et al., 2005; Martin, 1990). Due to expanded dust production areas, greater entrainment capabilities (drier soils and higher winds) and greater transport capacity due to less efficient washout (Muhs, 2013; Tegen and Kohfeld, 2006), total dust input to the glacial ocean was 2–10 times higher than modern deposition rates. We assume that even if loci of dust production are variable, the solubility and mean isotopic composition (*i.e.* −0.67 ± 0.45; Table 1) of the dust as estimated above are invariant.

5.1.3. Impact of glacial climate on the river sediment flux and δ^{30}Si

The boundary conditions that control river sediment export (*e.g.* temperature, precipitation, glacial activity and basin area) change over glacial cycles. Using U-series disequilibria, Dosseto et al. (2010) argue that sediment storage times in the Murrumbidgee River catchment, Australia, reached a minimum at the LGM due to the lack of stabilising influence from vegetation. Some larger rivers have sediment deliveries buffered by their alluvial plains on timescales as long as Quaternary glacial cycles (Métivier and Gaudemer, 1999), although this does not apply to all large rivers (Clift and Giosan, 2014). Even small mountain catchments can buffer sediment delivery on millennial timescales (Blöthe and Korup, 2013), introducing inertia into river system sediment fluxes. Glaciers and ice-sheets produce large amounts of finely ground glacial flour, but the extent to which this contributes to enhanced sediment fluxes rather than providing for a potential post-glacial pulse (Vance et al., 2009) is unclear. Modelling studies in both the Po River basin, northern Italy (Kettner and Syvitski, 2009), and the Waipaoa River, New Zealand (Upton et al., 2013), driven by temperature, precipitation, catchment size and an index of erodability suggest enhanced LGM fluxes relative to modern (preindustrial) fluxes. Overall, we consider that the net sediment load carried by rivers at the LGM was between 1 and 2× modern (preindustrial) values. We make the simplifying assumption that the percentage of this sediment liable to dissolve was a constant fraction, and we assume no post-glacial sediment pulses or lags, and that it had a constant δ^{30}Si.

5.2. Impact of continental ice-sheets on land-to-ocean Si fluxes

Subglacial and periglacial silicate weathering is different in style to subaerial weathering. Analysis of subglacial streams shows that silicate weathering tends to be more congruent, as evidenced by high Ge/Si (approaching the Ge/Si ratio of bedrock) and elemental stoichiometries (Tranter, 2005), and tends to be driven by acidity not sourced from atmospheric carbon (Anderson, 2005; Wadham et al., 2010). The few investigations of DSi δ^{30}Si in glaciated catchments (Georg et al., 2007a; Opfergelt et al., 2013) show that these tend to be low δ^{30}Si rivers that approach the parent material isotopic composition. Therefore, a world with increased sub- or peri-glacial solute generation could perhaps be expected to introduce low δ^{30}Si DSi. Opfergelt et al. (2013) found a difference in δ^{30}Si of 0.8‰ between glaciated and non-glaciated catchments in Iceland and estimated a net decrease in river δ^{30}Si of 0.12‰ due to the presence of the high-latitude ice sheets, mountain ice-caps and valley glaciers, which we retain here.

5.3. Impact of lowered sea-level on land-to-ocean Si fluxes

At the LGM, global eustatic sea levels were approximately 130 m lower as a result of water storage in the polar ice caps (Lambeck et al., 2014). This may affect the inputs to the global ocean and ocean Si cycling in at least three ways: i) a reduction in the 'fluvial filtering' of land to ocean fluxes, ii) the exposure of new land surface to subaerial weathering and remobilisation of 'old' BSi, with an associated reduction in the area of continental shelf available for neritic BSi sedimentation, and iii) alteration to groundwater flow dynamics.

5.3.1. DSi and the fluvial filter: alluvial plains, estuaries and lakes

The land-to-ocean DSi flux must pass through a series of biogeochemically reactive systems – wetlands, lakes, estuaries, etc. – that act as a 'fluvial-filter' (Billen et al., 1991; Meybeck and Vörösmarty, 2005). The base level of a river system is the lowest level to which it can be subaerially eroded, usually sea level. In response to a sea-level change and therefore a channel shortening or lengthening, a river network can aggrade or incise to adjust towards a new equilibrium profile, although the nature of the adjustment depends on shelf and channel gradients, sediment supply, stream power, etc. A full discussion of fluvial responses to base-level change is beyond the scope of this paper (reviews can be found in Blum and Törnqvist, 2000 and Schumm, 1993). However, we speculate that water/sediment interaction times in alluvial plains were lower at the LGM because of the lowered base-level, a suggestion advanced previously (Lupker et al., 2013).

In the Ganges basin today, rivers partially or completely draining the alluvial plain have DSi δ^{30}Si (typically >2‰) consistently and substantially higher than rivers draining solely the Himalaya (around 1‰) (Fontorbe et al., 2013; Frings et al., 2015). The silicon isotope composition (1.69‰) at the most downstream point reflects a conservative mixing of the upstream tributaries, meaning the presence of alluvial plain derived DSi pushes the δ^{30}Si of exported DSi higher by around 0.7‰ in the Ganges. As suggested above, δ^{30}Si from alluvial plain streams are high because sediment/water interaction times are sufficiently long to promote clay formation. If the interaction time between sediment and water is reduced, then we can speculate that secondary mineral formation will be reduced, with a correspondingly lower exported δ^{30}Si. We speculate that this could cause the mean river DSi δ^{30}Si to decrease by up to 0.2‰.

Lakes also act as biogeochemical reactors, converting some fraction of inflowing DSi into BSi and burying it in their sediments (Frings et al., 2014a; Harrison et al., 2012). This retention must shift δ^{30}Si of the residual DSi higher (Frings et al., 2014a; Hughes et al., 2012). Two global estimates of the magnitude of DSi retention in lakes arrived at similar values of ~25% of the river DSi flux (Frings et al., 2014a; Harrison et al., 2012), meaning that δ^{30}Si of river DSi is about 0.2‰ higher than in a hypothetical lake-free world, assuming a BSi production fractionation of −1.1‰ (Fig. 2). Many lakes today are glacial relics (Hutchinson, 1957), formed by glacial scouring or in dead-ice pits. This implies that during glacial periods there were fewer lakes and less DSi retention, so therefore less fractionation, perhaps compounded by decreased productivity (and therefore less efficient retention) in cooler climates. Overall, a reduced lake sink may constitute a further lowering of fluvial δ^{30}Si by *ca.* 0.1‰ in glacial periods.

Estuaries provide a final example of how a less efficient fluvial filter may have altered river Si fluxes on millennial timescales. Estuaries are of interest since they are features of periods of transgressive sea level (Weiss et al., 2015; Kennett, 1982). If these environments are acting as efficient particle or solute filters today (Section 4.1.3), we can expect them to behave differently (*i.e.* a much reduced filtering capacity) during the LGM sea level lowstand when river discharge into the ocean was mostly direct (Kennett, 1982). Taking the estimated isotopic impact of estuarine DSi retention (~0.1‰; Section 4.1.4), a near cessation of estuarine Si filtering associated with more direct riverine discharge to the ocean could conceivably lower the net δ^{30}Si of river DSi entering the open ocean by ~0.1‰ — assuming a BSi production fractionation of −1.1‰ (Fig. 2).

5.3.2. Exposure of continental shelf

BSi accumulation rates on continental shelves are high (~1.8×10^{12} mol yr^{-1}) because of high production rates (due to proximity to continental nutrients) and higher preservation efficiencies (due to shorter water column residence time and higher sedimentation rates) (DeMaster, 2002). This means that there are massive pools of BSi that could potentially become available to subaerial weathering during sea level lowstands. The δ^{30}Si of this is unknown; we speculate it could alter the mean δ^{30}Si of river DSi by ±0.1‰.

5.3.3. Potential modification of submarine groundwater discharge at the LGM

A lowering of base level both allows for greater freshwater storage in continental aquifers (Adkins et al., 2002) and increases the hydraulic gradient, which may be expected to increase the glacial submarine groundwater discharge (SGD) flux relative to today. To our knowledge, this has never been quantified. Global precipitation was lower at the LGM, but rates of evaporation also declined, meaning discharge remained relatively constant (Kump and Alley, 1994; Jones et al., 2002). However, it is possible that the partitioning of this discharge between SGD and rivers changed. We incorporate this into our scenarios whereby a glacial SGD increase of between 1 and 2× modern values is counterbalanced by a decrease in river runoff of the same magnitude; the δ^{30}Si of SGD is held constant.

5.4. Impact of altered vegetation zonation on land-to-ocean Si fluxes

At the LGM, there was a general equatorward contraction in the zonation of vegetation communities towards lower altitudes and latitudes, and an expansion of grasslands at both low and high latitudes (Harrison and Prentice, 2003). Given that distinctive Si cycles exist in these biomes, could this play a role? It is unclear to what extent there are systematic differences in silicate weathering rates beneath various biomes. In the absence of clear evidence, we assume that the latitudinal contraction and expansion of vegetation ranges characteristic of the Quaternary glacial cycles was not associated with a net change in the rate of the solubilisation of Si from bedrock at a global scale beyond that included in our ±20% DSi flux range (Section 5.1.1).

Vegetation pattern changes might alter the DSi exported from catchments *via* a change in Si cycling at an ecosystem level (Conley and Carey, 2015). The ratio of export of fractionated material to initial solubilisation from bedrock is a key control on the silicon isotope composition of river water (Section 3; Bouchez et al., 2013). Therefore if a larger fraction of the total Si exported is detrital biogenic opal or other secondary (alumino)silicates then the degree of fractionation relative to bedrock of the residual DSi should be more pronounced. Vegetation and its associated fungal and bacterial communities are key players in soil/clay formation; it is likely that some biomes are more efficient at producing secondary solids than others, but we are currently unable to evaluate this. Related, some ecosystems may export more Si as biogenic Si. Two lines of evidence suggest that this is not an important mechanism of change over G–IG cycles. Firstly, the biogenic component is generally a small fraction of the total of secondary Si phases produced and exported, which tend to be dominated by clay minerals (Section 3). Secondly, an assumption inherent in the preceding discussion (Section 5.2) is that the majority of BSi carried by rivers dissolves upon entry to seawater, such that it can have minimal net effect on the δ^{30}Si of Si delivered to the ocean.

A final mechanism whereby vegetation zonation may alter land-to-ocean Si fluxes is through transient changes in the size of the ecosystem Si pool. Although our understanding of terrestrial Si cycling is still in its infancy (Conley, 2002; Struyf and Conley, 2012), some aspects are reasonably well established. We know that terrestrial ecosystems develop a pool of Si in the soil–plant system that is composed of biogenic silica (BSi; mostly phytoliths) and its diagenetic products together with amorphous Si phases formed purely pedogenically (Barão et al., 2015; Sommer et al., 2006), and that this pool is isotopically distinct, being depleted in the heavy ^{30}Si (Cornelis et al., 2010, 2011; Vandevenne et al., 2015). We know that just considering the upper portion of a soil profile, this pool can be orders of magnitude larger than the annual Si export from a system (Struyf et al., 2010a,b). It has recently been estimated at 8250×10^{12} mol, *i.e.* ~1000 × annual DSi export (Laruelle et al., 2009) and ~100 × annual BSi production by terrestrial vegetation (Carey and Fulweiler, 2012). Finally, we know that the size of this pool varies among different ecosystems (summarised in Alfredsson et al., 2015), such that when land-cover changes the pool will aggrade or be depleted to reach a new steady state commensurate with the rate of input and the recycling efficiency (Clymans et al., 2011; Struyf et al., 2010b). There is therefore the potential for a transient increase or decrease in river DSi fluxes and/or associated changes in δ^{30}Si as the pool aggrades or depletes. At local scales, the build-up or depletion of this soil–plant ASi pool may be key in interpreting lacustrine δ^{30}Si records (Street-Perrott et al., 2008; Swann et al., 2010). One key unknown relates to the timescale of adjustment to a new steady-state. Although

Table 2
Summary of plausible changes to the magnitude and/or Si isotopic composition of dissolved Si inputs to the ocean, for the LGM relative to today.

Altered flux	Mechanism for alteration	Change in associated DSi flux	Change in associated δ^{30}Si (‰)
River DSi	Altered weathering regimes	±20%	−0.45 to +0.05
	Subglacial weathering		−0.15 to 0
	Lesser lake Si retention		−0.10 to 0
	Less alluvial plain interaction		−0.10 to 0.1
	Remobilisation of continental shelf BSi deposits		−0.10 to 0
	Reduced estuarine filter	0–10%[a]	−0.10 to 0[a]
	Net:	−20 to +30%	−1.00 to +0.05
Dust	Greater dust generation; less efficient continental rainout	2–10×	Constant
River SPM	Increased glacial flour production, less vegetation stabilisation	1–2×	Constant
SGD	Greater groundwater flow due to greater hydraulic head	1–2×	Constant

[a] Assumed to co-vary.

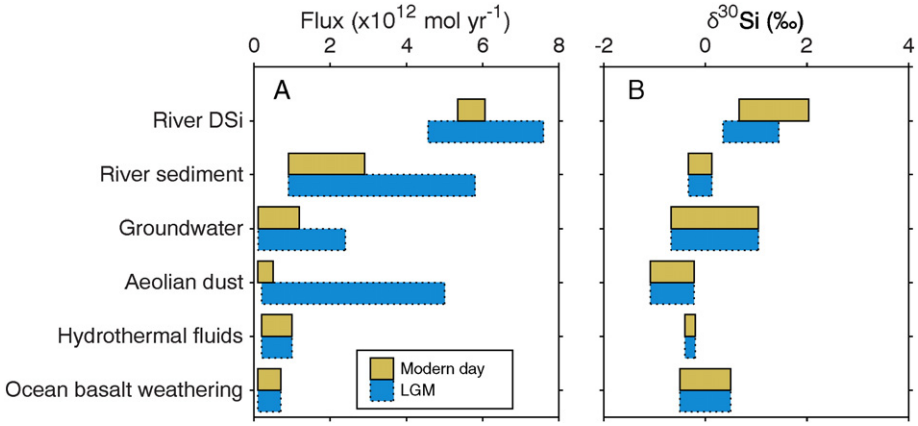

Fig. 10. A visual depiction of potential changes in the magnitudes (A) and δ^{30}Si (B) of DSi fluxes to the ocean between modern day (brown boxes) and LGM (blue boxes with dotted outline). The figure emphasises that the most likely mechanism of alterating the glacial ocean Si cycle is *via* a change in the relative importance of the individual fluxes, rather than *via* a change in their δ^{30}Si.

there is little evidence available, estimates of adjustment times span decadal to centennial timescales (Conley et al., 2008; Clymans et al., 2011; Struyf et al., 2010b), less than the multi-millennial perturbations required to impact the whole-ocean Si cycle. This can also be viewed in another, simpler way: the estimate of the size of the continental ASi pool (*i.e.* 8.25×10^{15} mol) is 'only' about 7% of the ocean DSi inventory (112×10^{15} mol) — too small to impact ocean δ^{30}Si on long timescales.

5.5. Synthesis of potential changes

A summary of these mechanisms for change, together with estimates of their impact on the Si flux magnitude and isotope composition, is presented in Table 2 and graphically in Fig. 10. Overall, this review suggests that the total inputs of DSi to the ocean have declined slightly from the LGM to today, and that the weighted δ^{30}Si of these inputs may have been up to 1‰ lower at the LGM, larger than the changes envisaged by previous work (Opfergelt et al., 2013; Georg et al., 2009a).

6. Manifestation of continental variability in the ocean Si cycle

Simple mass-balance calculations suggest that changes of >0.50‰ in river DSi δ^{30}Si alone are necessary to approach the level of variability observed in BSi (0.5 to 1‰). The synthesis above suggests changes of this magnitude are plausible, especially when considered in tandem with changing dust and groundwater fluxes and a reduced fluvial filter efficiency. If our analysis (Table 2) is correct in suggesting that a net change in the input weighted δ^{30}Si of ≥0.5‰ is plausible, then how rapidly is this observed in the ocean sediment record? Two studies have touched on this question before. One did not consider a time dependent aspect (Opfergelt et al., 2013). The second (Georg et al., 2009a) used a two-box model to resolve the time dependency and concluded that while δ^{30}Si of BSi did change, the magnitude and speed of this change was insufficient to be of interest. However, they considered only a variable SGD flux and held all other parameters constant.

Models of varying complexity have been used to investigate aspects of the ocean Si cycle. The simplest models have a limited number of boxes (De La Rocha and Bickle, 2005; Yool and Tyrrell, 2003, 2005; Laruelle et al., 2009; Bernard et al., 2010; de Souza et al., 2012; Reynolds,

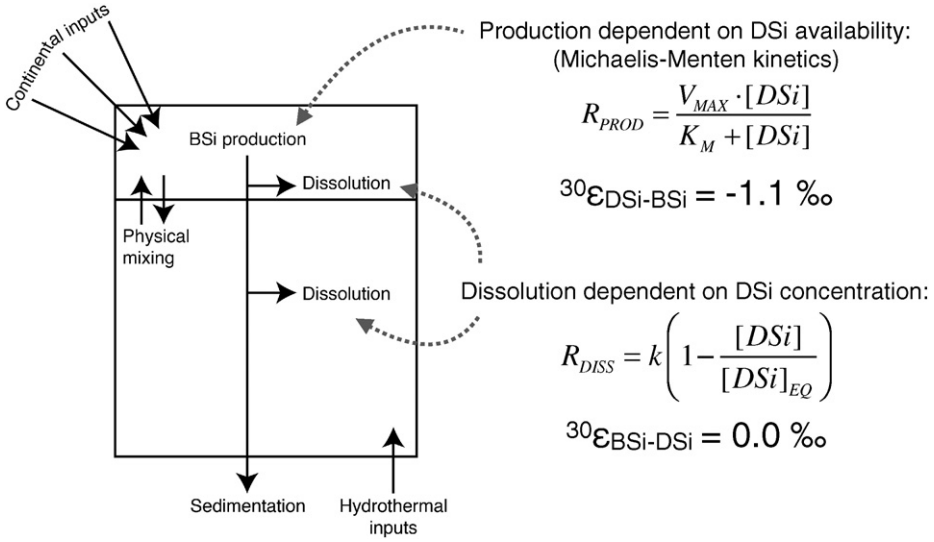

Fig. 11. Schematic of box model used to test ocean response to perturbations to input fluxes, showing both mass fluxes and associated fractionations, modified from De La Rocha and Bickle (2005). DSi inputs are prescribed independently into both the upper euphotic box (riverine, aeolian, and groundwater fluxes) and the deep ocean box (hydrothermal fluid recirculation). Si is transferred between the boxes by biological production, settling and dissolution, and physical mixing (upwelling and downwelling). See main text for more details.

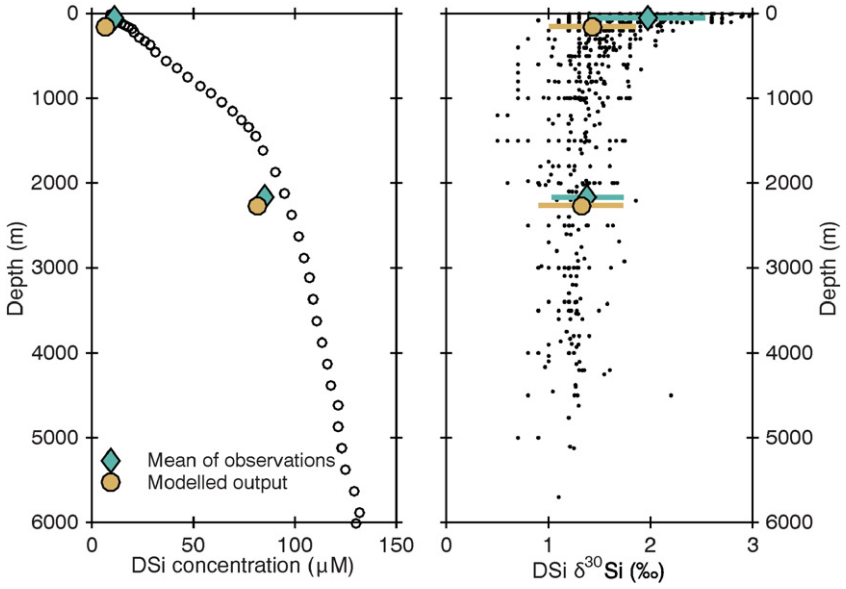

Fig. 12. Comparison of model output (brown circles) for the present day (parameters as in Table 1 and Supplementary data) with observational data (black dots, means given as green diamonds). DSi data averaged by depth from the global climatology of Gouretski and Koltermann (2004). Ocean δ^{30}Si data from literature compilation from all ocean basins (CDLR, unpublished compilation).

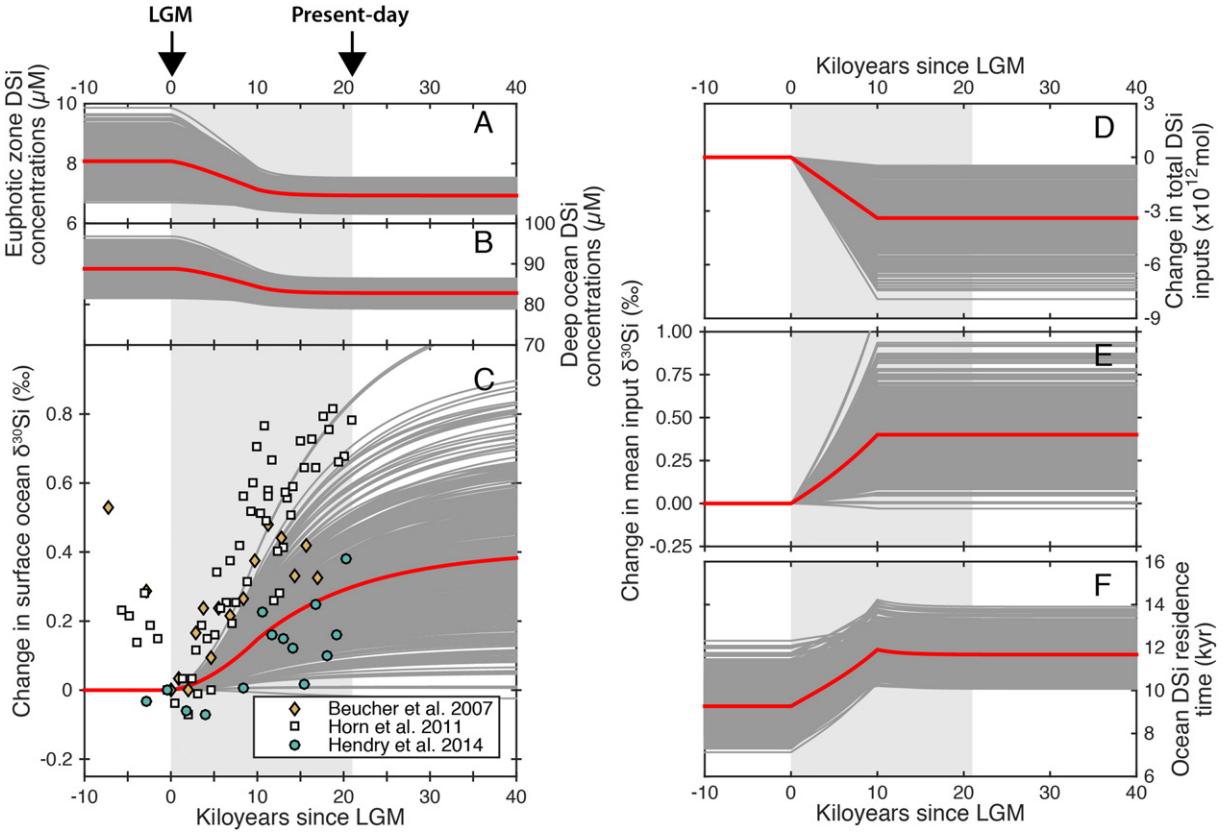

Fig. 13. Potential impact of changing land-to-ocean Si fluxes on millennial timescales on ocean Si cycling, as simulated by a two-box model. All results generated using 500 iterations (each light grey line represents one iteration), each representing one ensemble of input parameters randomly selected from the range of plausible values in Tables 1 and 2. See main text for details. A: Change in surface-water (upper 100 m) DSi concentrations in response to imposed input changes. B: Change in deep ocean (below 100 m) DSi concentrations in response to imposed input changes. C: Isotopic response of surface ocean DSi. Each iteration is standardised to a LGM baseline derived from a 50,000 yr spin-up period, in order to show the contrast between simulated glacial and modern oceans. Three representative downcore δ^{30}Si profiles from the sub-Antarctic Indian Ocean (Beucher et al. (2007), the Southern Ocean (Horn et al., 2011) and the North Atlantic (Hendry et al., 2014) are shown for comparison, also standardised to the δ^{30}Si of the sample nearest 21 ka, with the published age-models used as provided. D: Change in the sum of all input fluxes ($\times 10^{12}$ mol yr^{-1}), standardised to each iteration's LGM value. E: Change in the weighted mean δ^{30}Si of all DSi inputs to the ocean, standardised to each iteration's LGM value. F: Modelled Si residence time in the global ocean (total DSi inventory/annual DSi inputs).

2009; Nelson et al., 1995; Sutton et al., 2010; Ridgwell et al., 2002). More complex ocean general circulation models (GCMs) have also proved extremely insightful (*e.g.* Bernard et al., 2011; Wischmeyer et al., 2003), but simple box models have the advantage that many ensembles of input parameters can be tested to robustly assess model sensitivity and identify magnitudes and timescales of change.

Here, we use a simple two-box model modified from De La Rocha and Bickle (2005). The aim of this model is not to reproduce the exact response of the ocean Si cycle to perturbations but rather to assess the magnitude and timescales characteristic of ocean Si responses, and potential visibility in sedimentary record of changes to input fluxes. The model is modified slightly from that described in De La Rocha and Bickle (2005) and shown in Fig. 11. This simple approach captures the key features of the modern ocean Si cycle (Fig. 13), namely lower DSi, higher δ^{30}Si surface waters and higher DSi, lower δ^{30}Si deep waters, with a total DSi residence time (mass/inputs) of ~12 ka. The main modifications from the original De La Rocha and Bickle (2005) model are the incorporation of a DSi concentration dependency of BSi production and dissolution. The model and its parameterisation are described more fully in the Supplementary data. We use multiple model iterations with different flux parameterisations to allow us to assess model sensitivity and to account for our poor knowledge of modern DSi fluxes and even poorer knowledge of the palaeo-fluxes. (See Fig. 10.)

Both the magnitude and the isotopic composition of the input fluxes are varied over the course of a model run. For each iteration, values for the modern input fluxes and δ^{30}Si are randomly chosen from within the values and uncertainties given in Table 1. The LGM input values are then defined as a function of their deviation from the modern values, selected randomly from within the estimates in Table 2. The model is then spun-up to near equilibrium (50,000 model years) with the LGM values, then run from this baseline for a further 50,000 years, with all changes from LGM values to modern values conservatively assumed to occur progressively over a 10 ka deglacial period, *i.e.* assuming a monotonic climate transition. A series of sensitivity tests described in the Supplementary data demonstrate that the results described below are robust to changes in parameterisation.

6.1. Box model results

When the prescribed changes (Table 2, Fig. 10) are imposed on the model-ocean, BSi production and dissolution adjust on the timescale of ocean mixing (1000 years) to maintain steady-state and keep the sedimentation of BSi equal to the total DSi inputs. Because of this, from the LGM to the modern day, the residence time of DSi, BSi production and dissolution fluxes, preservation efficiency and DSi concentrations were all relatively invariant. Fig. 13a–b shows the change in modelled DSi concentrations from each LGM iteration to a modern day value. These small changes observed, despite relatively large changes to the input fluxes, demonstrate a relative insensitivity of the marine Si cycle to perturbations. Feedbacks between production and dissolution act to ensure that the total inventory of Si in the ocean is relatively insensitive to input fluxes, a conclusion corroborated by previous work (Ridgwell et al., 2002).

In contrast, the δ^{30}Si of ocean DSi, and therefore the BSi produced from it, exhibits relatively large changes and takes multiple Si residence times (>40,000 years) to reach steady-state. The results presented in Fig. 13c shows the modelled change in δ^{30}Si of surface ocean DSi over a 50,000 yr simulation, standardised to the baseline ("LGM") value for each iteration. Note that because δ^{30}Si of BSi in the model is approximately a constant offset (*i.e.* −1.1‰) from the surface ocean DSi, and because we prescribe no fractionation during dissolution (Wetzel et al., 2014), the δ^{30}Si of BSi buried in marine sediments produces identical results. Likewise, including a fractionation during dissolution only affects the absolute δ^{30}Si values of the buried BSi, not the relative trends (see Supplementary data). The δ^{30}Si of deep-ocean DSi is similarly offset from the surface ocean DSi. In the 20,000 model years from LGM to present, δ^{30}Si of surface ocean DSi (or BSi) changes by between ~0.0 and 0.8‰, depending on the suite of input values chosen. This is a similar magnitude of total change, and at a similar rate, as measured in sedimentary BSi δ^{30}Si (Figs. 5 and 13). The results suggest that diatom δ^{30}Si does not necessarily reflect simply palaeoutilisation of DSi or the other factors invoked to explain downcore δ^{30}Si changes, including water-mass mixing or species-specific effects (Sutton et al., 2013). Instead, diatom δ^{30}Si since the LGM potentially represents both these factors *and* a variable δ^{30}Si of whole-ocean DSi.

Many of the parameter ensembles in Fig. 13 show little change, while some exhibit change in δ^{30}Si of up to 0.8‰. This differences are primarily due to the difference in importance the randomised parameter selection ascribes to the dust, SPM and SGD fluxes. Because the LGM values are defined relative to the modern values, the scenarios that call for values of dust, river sediment and groundwater fluxes towards the higher end of their possible values (Table 1) are especially sensitive to changes in their magnitude. Because these fluxes have distinctively low δ^{30}Si relative to river DSi, this implies that they could be key controls, and overlooked, controls on the ocean Si isotope budget, particularly in the glacial ocean. Yet these fluxes, together with the fluxes of DSi from seafloor alteration, remain understudied. Their magnitudes and isotopic compositions are often based on tenuous assumptions or extrapolations (Section 4). This is a knowledge gap that would be relatively simple to address, and could be a future research priority.

The intention of this exercise is to demonstrate the potential for whole ocean shifts in δ^{30}Si of DSi rapid enough to be relevant for interpretation of downcore δ^{30}Si-BSi over glacial–interglacial cycles. Many processes cannot be incorporated. For example, the model clearly cannot capture the complexities of ocean circulation and the spatial distribution of marine DSi and δ^{30}Si, which is also a contributory factor to downcore δ^{30}Si records (Hendry and Brzezinski, 2014). Future research could focus on better constraining the magnitude of fluctuations in Si fluxes and isotopic compositions, and on more mechanistic modelling of the ocean Si cycle. Nevertheless, with a reasonable range of input parameters, our synthesis suggests that the continental Si cycle is directly responsible for somewhere between 10 and 100% of the well-established LGM-modern trend observed in marine δ^{30}Si records (Fig. 10). Importantly, the higher frequency (*i.e.* sub-millennial) variability, which is a feature of many records (*e.g.* Hendry et al., 2014; Hendry et al., 2016; Horn et al., 2011) is *not* explainable by such a whole-ocean mechanism and must instead reflect internal ocean circulation or productivity dynamics.

6.2. Implications of whole-ocean changes in δ^{30}Si of DSi

Any whole-ocean, long-term trend in DSi δ^{30}Si driven by a variable continental cycle should be detrended from BSi records before interpretation of palaeo-nutrient utilisation. As an example of an application of δ^{30}Si of BSi to palaeoenvironmental questions that may require reinterpretation, we highlight the issue of explaining changes in G–IG atmospheric CO_2. An outstanding question in the geosciences is the cause of the *ca.* 100 ppmv lower CO_2 concentrations at the LGM relative to the preindustrial world (Sigman and Boyle, 2000). As the largest carbon reservoir at the Earth's surface, the ocean must be involved in sequestering atmospheric carbon in the deep ocean during glacial periods, although a compelling explanation has thus far been elusive. One body of work has focused on increased siliceous productivity as a contributory mechanism (*e.g.* Harrison, 2000; Brzezinski et al., 2002; Matsumoto et al., 2002; see Hendry and Brzezinski, 2014 for a review). Testing these hypotheses hinges on demonstrating whether, and where, siliceous productivity increased at the LGM, and so downcore silicon isotope records (Fig. 5) have been an important part of evaluating these hypotheses. Accounting for the existence of a whole-ocean trend would tend to lessen the difference in DSi utilisation recorded in diatom δ^{30}Si between the LGM and modern oceans. In general, this weakens support for the family of hypotheses that invoke biosiliceous

productivity shifts as a mechanism to alter atmospheric CO_2, though it should be noted that these hypotheses often require upwelling/circulation changes not resolvable at a global scale (Hendry and Brzezinski, 2014).

Quantifying such a whole ocean trend should be a research priority, and could be achieved *via* two approaches. First, *via* more sophisticated modelling approaches than that employed here, perhaps driven by reconstructions of river DSi δ^{30}Si inferred from river delta sedimentary records, improved dust deposition fields, etc. Second, *via* measurements of δ^{30}Si over a glacial–interglacial cycle from an archive/proxy sensitive to whole-ocean δ^{30}Si changes, but insensitive to changing DSi concentration or utilisation. We suggest such an archive may be found in deep-sea siliceous sponges between 30° and 60° N in the Pacific. Here, DSi concentrations are among the highest observed in the global ocean (~170 μM), owing to its location at the end of the thermohaline 'conveyor belt.' Water here is among the oldest in the global ocean, and has had the longest time to accumulate regenerated Si from dissolution of BSi produced in surface waters (Sarmiento and Gruber, 2006). Because the relationship between siliceous sponge silicon isotope fractionation and ambient DSi concentrations plateaus at high DSi (Section 2.3), sponges consistently bathed in ≫100 μM DSi should exhibit more-or-less constant fractionation, meaning any variability must reflect instead changes in δ^{30}Si of the ambient DSi.

7. Conclusions and future directions

The fluxes of Si from land to ocean provide the majority of Si for the ocean Si cycle, and they are variable in terms of both magnitude and isotopic composition. While the ~12 ka residence time of DSi in the modern ocean buffers it against external forcing on short timescales, persistent changes to the inputs over millennia could theoretically produce a whole-ocean δ^{30}Si shift. Indeed, the consistency among different ocean basins of changes in δ^{30}Si from biogenic silica (BSi) over the last few glacial cycles hints at such a shift. These records document somewhere between 0.5 and 1‰ variability between low glacial δ^{30}Si and higher interglacial δ^{30}Si, which is classically interpreted in terms of palaeoproductivity. Given that the majority of all Si in the ocean originally derives from the continents, at least some of this variation may in fact reflect varying continental processes. A glacial continental Si cycle likely differs from the modern one, and we suggest that many processes operating together can cumulatively lower the mean δ^{30}Si of Si entering the ocean by up to 1‰. These include alterations to the rate and style of continental silicate weathering, less efficient continental and estuarine filtering of river fluxes, and increased dust and groundwater fluxes. A simple box-model suggests that these changes, prescribed gradually over the entire deglaciation, can produce a whole ocean δ^{30}Si increase of comparable rate, magnitude and timing to that recorded in sedimentary BSi. If correct, this implies that we may need to revisit some interpretations of the glacial–ocean Si cycle. It also suggests that the continental Si cycle should not be neglected when interpreting pre-Quaternary long-term $\delta 30Si_{BSi}$ records from marine sediment records (Fontorbe et al., in review; Egan et al., 2013).

However, many aspects of the modern and the palaeo-Si cycles need to be better constrained. We still have only a poor understanding of the magnitude of most inputs of Si to the global ocean, and an even poorer understanding of the controls on their isotopic composition. Only when these are better understood will we be able to improve the estimates of the direction and magnitude of change over the glacial–interglacial cycles that characterise the late Quaternary. Future research could take a three-pronged approach of measuring, modelling and reconstructing:

1. *Measuring*. What are the modern inputs of DSi to the ocean? In particular, DSi from dissolution of aeolian dust and river sediment (particularly non-basaltic terrains), DSi from alteration of the oceanic crust (high and low temperature), and DSi from submarine groundwater discharge, all need better constraining. The role of estuaries and the coastal zone *sensu lato*, in scavenging river Si fluxes also needs better quantification.
2. *Modelling*. Especially of the potential role for both transient and persistent impacts of terrestrial vegetation on river Si fluxes, and more sophisticated ocean response models.
3. *Reconstructing*. Interrogation of well chosen archives can provide useful information. For example, detrital clays in sedimentary archives seem well placed to inform about continental weathering rates and intensities, while sponge spicules from some sites in the global ocean may document long-term whole-ocean δ^{30}Si changes.

Acknowledgements

This research was funded by the Knut & Alice Wallenberg Foundation and the Swedish Research Council (2010–4696 and 2014–5910). We thank Kate Hendry for helpful comments on an earlier version of this manuscript, and Paul Savage and an anonymous reviewer for providing useful, constructive and insightful reviews.

Appendix A. Supplementary data

Supplementary data to this article can be found online at http://dx.doi.org/10.1016/j.chemgeo.2016.01.020.

References

Abraham, K., Opfergelt, S., Fripiat, F., Cavagna, A.J., de Jong, J.T.M., Foley, S.F., Andre, L., Cardinal, D., 2008. delta Si-30 and delta Si-29 determinations on USGS BHVO-1 and BHVO-2 reference materials with a new configuration on a Nu plasma multi-collector ICP-MS. Geostand. Geoanal. Res. 32, 193–202.

Abelmann, A., Gersonde, R., Knorr, G., Zhang, X., Chapligin, B., Maier, E., Esper, O., Friedrichsen, H., Lohmann, G., Meyer, H., Tiedemann, R., 2015. The seasonal sea-ice zone in the glacial Southern Ocean as a carbon sink. Nat. Commun. 6.

Adkins, J.F., McIntyre, K., Schrag, D.P., 2002. The salinity, temperature, and δ^{18}O of the Glacial Deep Ocean. Science 298, 1769–1773.

Alfredsson, H., Hugelius, G., Clymans, W., Stadmark, J., Kuhry, P., Conley, D.J., 2015. Amorphous silica pools in permafrost soils of the Central Canadian Arctic and the potential impact of climate change. Biogeochemistry 1–19.

Alleman, L.Y., Cardinal, D., Cocquyt, C., Plisnier, P.D., Descy, J.P., Kimirei, I., Sinyinza, D., Andre, L., 2005. Silicon isotopic fractionation in Lake Tanganyika and its main tributaries. J. Great Lakes Res. 31, 509–519.

Aller, R.C., 2014. 8.11 — Sedimentary diagenesis, depositional environments, and benthic fluxes. In: Turekian, H.D.H.K. (Ed.), Treatise on Geochemistry, second ed. Elsevier, Oxford, pp. 293–334.

Allison, M., Kuehl, S., Martin, T., Hassan, A., 1998. Importance of flood-plain sedimentation for river sediment budgets and terrigenous input to the oceans: insights from the Brahmaputra–Jamuna River. Geology 26, 175–178.

Anderson, S.P., 2005. Glaciers show direct linkage between erosion rate and chemical weathering fluxes. Geomorphology 67, 147–157.

Armytage, R., Georg, R., Savage, P., Williams, H., Halliday, A., 2011. Silicon isotopes in meteorites and planetary core formation. Geochim. Cosmochim. Acta 75, 3662–3676.

Bagard, M.-L., Chabaux, F., Pokrovsky, O.S., Viers, J., Prokushkin, A.S., Stille, P., Rihs, S., Schmitt, A.-D., Dupré, B., 2011. Seasonal variability of element fluxes in two Central Siberian rivers draining high latitude permafrost dominated areas. Geochim. Cosmochim. Acta 75, 3335–3357.

Barão, L., Clymans, W., Vandevenne, F., Meire, P., Conley, D.J., Struyf, E., 2014. Pedogenic and biogenic alkaline-extracted silicon distributions along a temperate land-use gradient. Eur. J. Soil Sci. 65, 693–705.

Barão, L., Vandevenne, F., Clymans, W., Frings, P., Ragueneau, O., Meire, P., Conley, D.J., Struyf, E., 2015. Alkaline-extractable silicon from land to ocean: a challenge for biogenic silicon determination. Limnol. Oceanogr. Methods 13, 329–344.

Basile-Doelsch, I., Meunier, J.D., Parron, C., 2005. Another continental pool in the terrestrial silicon cycle. Nature 433, 399–402.

Bern, C.R., Brzezinski, M.A., Beucher, C., Ziegler, K., Chadwick, O.A., 2010. Weathering, dust, and biocycling effects on soil silicon isotope ratios. Geochim. Cosmochim. Acta 74, 876–889.

Bernard, C.Y., Durr, H.H., Heinze, C., Segschneider, J., Maier-Reimer, E., 2011. Contribution of riverine nutrients to the silicon biogeochemistry of the global ocean — a model study. Biogeosciences 8, 551–564.

Bernard, C.Y., Laruelle, G.G., Slomp, C.P., Heinze, C., 2010. Impact of changes in river fluxes of silica on the global marine silicon cycle: a model comparison. Biogeosciences 7, 441–453.

Berner, R.A., Caldeira, K., 1997. The need for mass balance and feedback in the geochemical carbon cycle. Geology 25, 955–956.

Beucher, C.P., Brzezinski, M.A., Crosta, X., 2007. Silicic acid dynamics in the glacial sub-Antarctic: implications for the silicic acid leakage hypothesis. Glob. Biogeochem. Cycles 21.

Beucher, C.P., Brzezinski, M.A., Jones, J.L., 2008. Sources and biological fractionation of silicon isotopes in the Eastern Equatorial Pacific. Geochim. Cosmochim. Acta 72, 3063–3073.

Beusen, A.H.W., Bouwman, A.F., Dürr, H.H., Dekkers, A.L.M., Hartmann, J., 2009. Global patterns of dissolved silica export to the coastal zone: results from a spatially explicit global model. Glob. Biogeochem. Cycles 23, GB0A02.

Bien, G., Contois, D., Thomas, W., 1958. The removal of soluble silica from fresh water entering the sea. Geochim. Cosmochim. Acta 14, 35–54.

Billen, G., Lancelot, C., Meybeck, M., Mantoura, R., Martin, J.-M., Wollast, R., 1991. N, P and Si retention along the aquatic continuum from land to ocean. Ocean Margin Processes in Global Change 1. John Wiley & Sons, pp. 19–44.

Birke, M., Reimann, C., Demetriades, A., Rauch, U., Lorenz, H., Harazim, B., Glatte, W., 2010. Determination of major and trace elements in European bottled mineral water — analytical methods. J. Geochem. Explor. 107, 217–226.

Blecker, S.W., McCulley, R.L., Chadwick, O.A., Kelly, E.F., 2006. Biologic cycling of silica across a grassland bioclimosequence. Glob. Biogeochem. Cycles 20, GB3023.

Blöthe, J.H., Korup, O., 2013. Millennial lag times in the Himalayan sediment routing system. Earth Planet. Sci. Lett. 382, 38–46.

Blum, M.D., Törnqvist, T.E., 2000. Fluvial responses to climate and sea-level change: a review and look forward. Sedimentology 47, 2–48.

Bouchez, J., Gaillardet, J., von Blanckenburg, F., 2014. Weathering intensity in lowland river basins: from the Andes to the Amazon mouth. Procedia Earth Planet. Sci. 10, 280–286.

Bouchez, J., von Blanckenburg, F., Schuessler, J.A., 2013. Modeling novel stable isotope ratios in the weathering zone. Am. J. Sci. 313, 267–308.

Bouwman, A.F., Bierkens, M.F.P., Griffioen, J., Hefting, M.M., Middelburg, J.J., Middelkoop, H., Slomp, C.P., 2013. Nutrient dynamics, transfer and retention along the aquatic continuum from land to ocean: towards integration of ecological and biogeochemical models. Biogeosciences 10, 1–22.

Broecker, W., Peng, T., 1982. Tracers in the sea. Lamont-Doherty Geol. Obs., Palisades, NY (690 pp.).

Brzezinski, M.A., Pride, C.J., Franck, V.M., Sigman, D.M., Sarmiento, J.L., Matsumoto, K., Gruber, N., Rau, G.H., Coale, K.H., 2002. A switch from Si(OH)(4) to NO_3^- depletion in the glacial Southern Ocean. Geophys. Res. Lett. 29.

Burnett, W.C., Aggarwal, P.K., Aureli, A., Bokuniewicz, H., Cable, J.E., Charette, M.A., Kontar, E., Krupa, S., Kulkarni, K.M., Loveless, A., Moore, W.S., Oberdorfer, J.A., Oliveira, J., Ozyurt, N., Povinec, P., Privitera, A.M.G., Rajar, R., Ramessur, R.T., Scholten, J., Stieglitz, T., Taniguchi, M., Turner, J.V., 2006. Quantifying submarine groundwater discharge in the coastal zone via multiple methods. Sci. Total Environ. 367, 498–543.

Carbonnel, V., Vanderborght, J.-P., Lionard, M., Chou, L., 2013. Diatoms, silicic acid and biogenic silica dynamics along the salinity gradient of the Scheldt estuary (Belgium/The Netherlands). Biogeochemistry 113, 657–682.

Cardinal, D., Gaillardet, J., Hughes, H.J., Opfergelt, S., André, L., 2010. Contrasting silicon isotope signatures in rivers from the Congo Basin and the specific behaviour of organic-rich waters. Geophys. Res. Lett. 37, L12403.

Cardinal, D., Savoye, N., Trull, T.W., Dehairs, F., Kopczynska, E.E., Fripiat, F., Tison, J.L., Andre, L., 2007. Silicon isotopes in spring Southern Ocean diatoms: large zonal changes despite homogeneity among size fractions. Mar. Chem. 106, 46–62.

Cardinal, D., Alleman, L.Y., Dehairs, F., Savoye, N., Trull, T.W., André, L., 2005. Relevance of silicon isotopes to Si-nutrient utilization and Si-source assessment in Antarctic waters. Glob. Biogeochem. Cycles 19, GB2007.

Carey, J.C., Fulweiler, R.W., 2012. The terrestrial silica pump. PLoS One 7, e52932.

Cary, L., Alexandre, A., Meunier, J.D., Boeglin, J.L., Braun, J.J., 2005. Contribution of phytoliths to the suspended load of biogenic silica in the Nyong basin rivers (Cameroon). Biogeochemistry 74, 101–114.

Chakrabarti, R., Jacobsen, S.B., 2010. Silicon isotopes in the inner solar system: implications for core formation, solar nebular processes and partial melting. Geochim. Cosmochim. Acta 74, 6921–6933.

Chou, L., Wollast, R., 2006. Estuarine silicon dynamics. In: Ittekkot, D., Unger, C., Humborg, C., Tac An, N. (Eds.), The Silicon Cycle: Human Perturbations and Impacts on Aquatic Systems. Scope vol. 66, pp. 93–120.

Clarke, A., 1924. Data of Geochemistry. fifth ed. USGS, Washington (841 pp.).

Clift, P., Giosan, L., 2014. Sediment fluxes and buffering in the post-glacial Indus Basin. Basin Res. 26, 369–386.

Clymans, W., Struyf, E., Govers, G., Vandevenne, F., Conley, D.J., 2011. Anthropogenic impact on biogenic Si pools in temperate soils. Biogeosciences 8, 2281–2293.

Cockerton, H.E., Street-Perrott, F.A., Leng, M.J., Barker, P.A., Horstwood, M.S.A., Pashley, V., 2013. Stable-isotope (H, O, and Si) evidence for seasonal variations in hydrology and Si cycling from modern waters in the Nile Basin: implications for interpreting the Quaternary record. Quat. Sci. Rev. 66, 4–21.

Cockerton, H.E., Street-Perrott, F.A., Barker, P.A., Leng, M.J., Sloane, H.J., Ficken, K.J., 2015. Orbital forcing of glacial/interglacial variations in chemical weathering and silicon cycling within the upper White Nile basin, East Africa: stable-isotope and biomarker evidence from Lakes Victoria and Edward. Quat. Sci. Rev. 130, 57–71.

Colman, S.M., Bratton, J.F., 2003. Anthropogenically induced changes in sediment and biogenic silica fluxes in Chesapeake Bay. Geology 31, 71–74.

Conley, D.J., 1997. Riverine contribution of biogenic silica to the oceanic silica budget. Limnol. Oceanogr. 42, 774–777.

Conley, D.J., 2002. Terrestrial ecosystems and the global biogeochemical silica cycle. Glob. Biogeochem. Cycles 16, 1121.

Conley, D.J., Likens, G.E., Buso, D.C., Saccone, L., Bailey, S.W., Johnson, C.E., 2008. Deforestation causes increased dissolved silicate losses in the Hubbard Brook Experimental Forest. Glob. Chang. Biol. 14, 2548–2554.

Conley, D.J., Malone, T.C., 1992. The annual cycle of dissolved silicate in Chesapeake Bay: implications for the production and fate of phytoplankton biomass. Mar. Ecol. Prog. Ser. 81, 121–128.

Conley, D.J., Carey, J.C., 2015. Biogeochemistry: silica cycling over geologic time. Nat. Geosci. 8, 431–432.

Cornelis, J.T., Weis, D., Lavkulich, L., Vermeire, M.-L., Delvaux, B., Barling, J., 2014. Silicon isotopes record dissolution and re-precipitation of pedogenic clay minerals in a podzolic soil chronosequence. Geoderma 235–236, 19–29.

Cornelis, J.T., Delvaux, B., Cardinal, D., Andre, L., Ranger, J., Opfergelt, S., 2010. Tracing mechanisms controlling the release of dissolved silicon in forest soil solutions using Si isotopes and Ge/Si ratios. Geochim. Cosmochim. Acta 74, 3913–3924.

Cornelis, J.T., Delvaux, B., Georg, R.B., Lucas, Y., Ranger, J., Opfergelt, S., 2011. Tracing the origin of dissolved silicon transferred from various soil–plant systems towards rivers: a review. Biogeosciences 8, 89–112.

Dai, A., Trenberth, K.E., 2002. Estimates of freshwater discharge from continents: latitudinal and seasonal variations. J. Hydrometeorol. 3, 660–687.

Davis, S.N., 1964. Silica in streams and ground water. Am. J. Sci. 262, 870–891.

De La Rocha, C.L., 2003. Silicon isotope fractionation by marine sponges and the reconstruction of the silicon isotope composition of ancient deep water. Geology 31, 423–426.

De La Rocha, C.L., 2006. The biological pump. Oceans Mar. Geochem. 6, 83–112.

De La Rocha, C.L., Bickle, M.J., 2005. Sensitivity of silicon isotopes to whole-ocean changes in the silica cycle. Mar. Geol. 217, 267–282.

De La Rocha, C.L., Brzezinski, M.A., DeNiro, M.J., 1997. Fractionation of silicon isotopes by marine diatoms during biogenic silica formation. Geochim. Cosmochim. Acta 61, 5051–5056.

De La Rocha, C.L., Brzezinski, M.A., DeNiro, M.J., 2000. A first look at the distribution of the stable isotopes of silicon in natural waters. Geochim. Cosmochim. Acta 64, 2467–2477.

De La Rocha, C.L., Brzezinski, M.A., DeNiro, M.J., Shemesh, A., 1998. Silicon-isotope composition of diatoms as an indicator of past oceanic change. Nature 395, 680–683.

De La Rocha, C.L., Bescont, P., Croguennoc, A., Ponzevera, E., 2011. The silicon isotopic composition of surface waters in the Atlantic and Indian sectors of the Southern Ocean. Geochim. Cosmochim. Acta 75, 5283–5295.

de Souza, G.F., Reynolds, B.C., Rickli, J., Frank, M., Saito, M.A., Gerringa, L.J.A., Bourdon, B., 2012. Southern Ocean control of silicon stable isotope distribution in the deep Atlantic Ocean. Glob. Biogeochem. Cycles 26, GB2035.

de Souza, G.F., Slater, R.D., Dunne, J.P., Sarmiento, J.L., 2014. Deconvolving the controls on the deep ocean's silicon stable isotope distribution. Earth Planet. Sci. Lett. 398, 66–76.

Delstanche, S., Opfergelt, S., Cardinal, D., Elsass, F., André, L., Delvaux, B., 2009. Silicon isotopic fractionation during adsorption of aqueous monosilicic acid onto iron oxide. Geochim. Cosmochim. Acta 73, 923–934.

Delvaux, C., Cardinal, D., Carbonnel, V., Chou, L., Hughes, H.J., André, L., 2013. Controls on riverine δ^{30}Si signatures in a temperate watershed under high anthropogenic pressure (Scheldt — Belgium). J. Mar. Syst. 128, 40–51.

Demarest, M.S., Brzezinski, M.A., Beucher, C.P., 2009. Fractionation of silicon isotopes during biogenic silica dissolution. Geochim. Cosmochim. Acta 73, 5572–5583.

DeMaster, D.J., 1981. The supply and accumulation of silica in the marine-environment. Geochim. Cosmochim. Acta 45, 1715–1732.

DeMaster, D.J., 2002. The accumulation and cycling of biogenic silica in the Southern Ocean: revisiting the marine silica budget. Deep-Sea Res. II Top. Stud. Oceanogr. 49, 3155–3167.

DePaolo, D.J., 2011. Surface kinetic model for isotopic and trace element fractionation during precipitation of calcite from aqueous solutions. Geochim. Cosmochim. Acta 75, 1039–1056.

Derry, L.A., Kurtz, A.C., Ziegler, K., Chadwick, O.A., 2005. Biological control of terrestrial silica cycling and export fluxes to watersheds. Nature 433, 728–731.

Ding, T., Jiang, M.S., Wan, D., Li, Y., Li, J., Song, H., Liu, Z., Yao, X., 1996. Silicon Isotope Geochemistry. Geological Publishing House, Beijing, China (125 pp.).

Ding, T., Wan, D., Bai, R., Zhang, Z., Shen, Y., Meng, R., 2005a. Silicon isotope abundance ratios and atomic weights of NBS-28 and other reference materials. Geochim. Cosmochim. Acta 69, 5487–5494.

Ding, T., Wan, D., Wang, C., Zhang, F., 2004. Silicon isotope compositions of dissolved silicon and suspended matter in the Yangtze River, China. Geochim. Cosmochim. Acta 68, 205–216.

Ding, T.P., Gao, J.F., Tian, S.H., Wang, H.B., Li, M., 2011. Silicon isotopic composition of dissolved silicon and suspended particulate matter in the Yellow River, China, with implications for the global silicon cycle. Geochim. Cosmochim. Acta 75, 6672–6689.

Ding, T.P., Ma, G.R., Shui, M.X., Wan, D.F., Li, R.H., 2005b. Silicon isotope study on rice plants from the Zhejiang Province, China. Chem. Geol. 218, 41–50.

Ding, T.P., Tian, S.H., Sun, L., Wu, L.H., Zhou, J.X., Chen, Z.Y., 2008. Silicon isotope fractionation between rice plants and nutrient solution and its significance to the study of the silicon cycle. Geochim. Cosmochim. Acta 72, 5600–5615.

Dosseto, A., Vigier, N., Joannes-Boyau, R., Moffat, I., Singh, T., Srivastava, P., 2015. Rapid response of silicate weathering rates to climate change in the Himalaya. Geochem. Perspect. Lett. 1, 10–19.

Dosseto, A., Hesse, P., Maher, K., Fryirs, K., Turner, S., 2010. Climatic and vegetation control on sediment dynamics during the last glacial cycle. Geology 38, 395–398.

Douthitt, C.B., 1982. The geochemistry of the stable isotopes of silicon. Geochim. Cosmochim. Acta 46, 1449–1458.

Dowling, C.B., Poreda, R.J., Basu, A.R., 2003. The groundwater geochemistry of the Bengal Basin: weathering, chemsorption, and trace metal flux to the oceans. Geochim. Cosmochim. Acta 67, 2117–2136.

Duce, R.A., Liss, P.S., Merrill, J.T., Atlas, E.L., Buat-Menard, P., Hicks, B.B., Miller, J.M., Prospero, J.M., Arimoto, R., Church, T.M., Ellis, W., Galloway, J.N., Hansen, L., Jickells, T.D., Knap, A.H., Reinhardt, K.H., Schneider, B., Soudine, A., Tokos, J.J., Tsunogai, S., Wollast, R., Zhou, M., 1991. The atmospheric input of trace species to the world ocean. Glob. Biogeochem. Cycles 5, 193–259.

Dupré, B., Dessert, C., Oliva, P., Goddéris, Y., Viers, J., François, L., Millot, R., Gaillardet, J., 2003. Rivers, chemical weathering and Earth's climate. Compt. Rendus Geosci. 335, 1141–1160.
Dupré, B., Gaillardet, J., Rousseau, D., Allègre, C.J., 1996. Major and trace elements of river-borne material: the Congo Basin. Geochim. Cosmochim. Acta 60, 1301–1321.
Dupuis, R., Benoit, M., Nardin, E., Méheut, M., 2015. Fractionation of silicon isotopes in liquids: the importance of configurational disorder. Chem. Geol. 396, 239–254.
Dürr, H.H., Laruelle, G.G., van Kempen, C.M., Slomp, C.P., Meybeck, M., Middelkoop, H., 2011a. Worldwide typology of nearshore coastal systems: defining the estuarine filter of river inputs to the oceans. Estuar. Coasts 34, 441–458.
Dürr, H.H., Meybeck, M., Hartmann, J., Laruelle, G.G., Roubeix, V., 2011b. Global spatial distribution of natural riverine silica inputs to the coastal zone. Biogeosciences 8, 597–620.
Egan, K.E., Rickaby, R.E.M., Leng, M.J., Hendry, K.R., Hermoso, M., Sloane, H.J., Bostock, H., Halliday, A.N., 2012. Diatom silicon isotopes as a proxy for silicic acid utilisation: a Southern Ocean core top calibration. Geochim. Cosmochim. Acta 96, 174–192.
Egan, K.E., Rickaby, R.E.M., Hendry, K.R., Halliday, A.N., 2013. Opening the gateways for diatoms primes Earth for Antarctic glaciation. Earth Planet. Sci. Lett. 375, 34–43.
Egge, J.K., Asknes, D.L., 1992. Silicate as regulating nutrient in phytoplankton competition. Mar. Ecol. Prog. Ser. 83, 281–289.
Ehlert, C., Grasse, P., Frank, M., 2013. Changes in silicate utilisation and upwelling intensity off Peru since the Last Glacial Maximum—insights from silicon and neodymium isotopes. Quat. Sci. Rev. 72, 18–35.
Ellwood, M.J., Wille, M., Maher, W., 2010. Glacial silicic acid concentrations in the Southern Ocean. Science 330, 1088–1091.
Engelstaedter, S., Tegen, I., Washington, R., 2006. North African dust emissions and transport. Earth Sci. Rev. 79, 73–100.
Engström, E., 2009. Fractionation of the stable silicon isotopes studied using MC-ICP-MS. Department of Chemical Engineering and Geosciences. Luleå University of Technology, Luleå.
Engström, E., Rodushkin, I., Ingri, J., Baxter, D.C., Ecke, F., Osterlund, H., Ohlander, B., 2010. Temporal isotopic variations of dissolved silicon in a pristine boreal river. Chem. Geol. 271, 142–152.
Engström, E., Rodushkin, I., Ohlander, B., Ingri, J., Baxter, D.C., 2008. Silicon isotopic composition of boreal forest vegetation in Northern Sweden. Chem. Geol. 257, 250–259.
Epstein, E., 1999. Silicon. Annu. Rev. Plant Physiol. Plant Mol. Biol. 50, 641–664.
Fitoussi, C., Bourdon, B., 2012. Silicon isotope evidence against an enstatite chondrite Earth. Science 335, 1477–1480.
Fitoussi, C., Bourdon, B., Kleine, T., Oberli, F., Reynolds, B.C., 2009. Si isotope systematics of meteorites and terrestrial peridotites: implications for Mg/Si fractionation in the solar nebula and for Si in the Earth's core. Earth Planet. Sci. Lett. 287, 77–85.
Fontorbe, G., De La Rocha, C.L., Chapman, H.J., Bickle, M.J., 2013. The silicon isotopic composition of the Ganges and its tributaries. Earth Planet. Sci. Lett. 381, 21–30.
Fontorbe, G., Frings, P.J., De La Rocha, C.L., Hendry, K.R., Conley, D., 2016. A silicon depleted North Atlantic since the Palaeogene: evidence from sponge and radiolarian silicon isotopes. Earth Planet. Sci. Lett. (in review).
Foster, G.L., Vance, D., 2006. Negligible glacial–interglacial variation in continental chemical weathering rates. Nature 444, 918–921.
Frings, P., Clymans, W., Jeppesen, E., Lauridsen, T., Struyf, E., Conley, D., 2014a. Lack of steady-state in the global biogeochemical Si cycle: emerging evidence from lake Si sequestration. Biogeochemistry 117, 255–277.
Frings, P.J., 2014. Integrating Fluvial Processes into the Global Si Cycle. Department of Geology. Lund University, Lund, p. 161.
Frings, P.J., Clymans, W., Conley, D.J., 2014b. Amorphous silica transport in the Ganges Basin: implications for Si delivery to the oceans. Procedia Earth Planet. Sci. 10, 271–274.
Frings, P.J., Clymans, W., Fontorbe, G., Gray, W., Chakrapani, G.J., Conley, D.J., De La Rocha, C.L., 2015. Silicate weathering in the Ganges alluvial plain. Earth Planet. Sci. Lett. http://dx.doi.org/10.1016/j.epsl.2015.06.049.
Frings, P.J., De La Rocha, C., Struyf, E., van Pelt, D., Schoelynck, J., Hudson, M.M., Gondwe, M.J., Wolski, P., Mosimane, K., Gray, W., Schaller, J., Conley, D.J., 2014c. Tracing silicon cycling in the Okavango Delta, a sub-tropical flood-pulse wetland using silicon isotopes. Geochim. Cosmochim. Acta 142, 132–148.
Fripiat, F., Cavagna, A.-J., Savoye, N., Dehairs, F., André, L., Cardinal, D., 2011. Isotopic constraints on the Si-biogeochemical cycle of the Antarctic zone in the Kerguelen area (KEOPS). Mar. Chem. 123, 11–22.
Fulweiler, R.W., Nixon, S.W., 2005. Terrestrial vegetation and the seasonal cycle of dissolved silica in a southern New England coastal river. Biogeochemistry 74, 115–130.
Gaillardet, J., Dupre, B., Allegre, C.J., Négrel, P., 1997. Chemical and physical denudation in the Amazon River Basin. Chem. Geol. 142, 141–173.
Gehlen, M., Heinze, C., Maier-Reimer, E., Measures, C., 2003. Coupled Al–Si geochemistry in an ocean general circulation model: a tool for the validation of oceanic dust deposition fields? Glob. Biogeochem. Cycles 17.
Geilert, S., Vroon, P.Z., Roerdink, D.L., Cappellen, P.V., van Bergen, M.J., 2014. Silicon isotope fractionation during abiotic silica precipitation at low temperatures: inferences from flow-through experiments. Geochim. Cosmochim. Acta 142, 95–114.
Geilert, S., Vroon, P.Z., Keller, N.S., Gudbrandsson, S., Stefánsson, A., van Bergen, M.J., 2015. Silicon isotope fractionation during silica precipitation from hot-spring waters: evidence from the Geysir geothermal field, Iceland. Geochim. Cosmochim. Acta 164, 403–427.
Georg, R.B., Reynolds, B.C., Frank, M., Halliday, A.N., 2006. Mechanisms controlling the silicon isotopic compositions of river waters. Earth Planet. Sci. Lett. 249, 290–306.
Georg, R.B., Reynolds, B.C., West, A.J., Burton, K.W., Halliday, A.N., 2007a. Silicon isotope variations accompanying basalt weathering in Iceland. Earth Planet. Sci. Lett. 261, 476–490.
Georg, R.B., Halliday, A.N., Schauble, E.A., Reynolds, B.C., 2007b. Silicon in the Earth's core. Nature 447, 1102–1106.
Georg, R.B., West, A.J., Basu, A.R., Halliday, A.N., 2009a. Silicon fluxes and isotope composition of direct groundwater discharge into the Bay of Bengal and the effect on the global ocean silicon isotope budget. Earth Planet. Sci. Lett. 283, 67–74.
Georg, R.B., Zhu, C., Reynolds, B.C., Halliday, A.N., 2009b. Stable silicon isotopes of groundwater, feldspars, and clay coatings in the Navajo Sandstone aquifer, Black Mesa, Arizona, USA. Geochim. Cosmochim. Acta 73, 2229–2241.
Gibbs, M.T., Kump, L.R., 1994. Global chemical erosion during the last glacial maximum and the present — sensitivity to changes in lithology and hydrology. Paleoceanography 9, 529–543.
Gislason, S.R., Oelkers, E.H., Snorrason, Á., 2006. Role of river-suspended material in the global carbon cycle. Geology 34, 49–52.
Gouretski, V., Koltermann, K.P., 2004. WOCE global hydrographic climatology. Ber. BSH 35, 1–52.
Griffiths, J.D., Barker, S., Hendry, K.R., Thornalley, D.J.R., van de Flierdt, T., Hall, I.R., Anderson, R.F., 2013. Evidence of silicic acid leakage to the tropical Atlantic via Antarctic Intermediate Water during Marine Isotope Stage 4. Paleoceanography 28, 307–318.
Guerzoni, S., Molinaroli, E., Rossini, P., Rampazzo, G., Quarantotto, G., De Falco, G., Cristini, S., 1999. Role of desert aerosol in metal fluxes in the Mediterranean area. Chemosphere 39, 229–246.
Guntzer, F., Keller, C., Meunier, J.-D., 2012. Benefits of plant silicon for crops: a review. Agron. Sustain. Dev. 32, 201–213.
Han, Q., Moore, J.K., Zender, C., Measures, C., Hydes, D., 2008. Constraining oceanic dust deposition using surface ocean dissolved Al. Glob. Biogeochem. Cycles 22.
Harrison, J.A., Frings, P.J., Beusen, A.H.W., Conley, D.J., McCrackin, M.L., 2012. Global importance, patterns, and controls of dissolved silica retention in lakes and reservoirs. Glob. Biogeochem. Cycles 26, GB2037.
Harrison, K.G., 2000. Role of increased marine silica input on paleo-pCO_2 levels. Paleoceanography 15, 292–298.
Harrison, S.P., Prentice, C.I., 2003. Climate and CO_2 controls on global vegetation distribution at the last glacial maximum: analysis based on palaeovegetation data, biome modelling and palaeoclimate simulations. Glob. Chang. Biol. 9, 983–1004.
Hendry, K.R., Brzezinski, M.A., 2014. Using silicon isotopes to understand the role of the Southern Ocean in modern and ancient biogeochemistry and climate. Quat. Sci. Rev. 89, 13–26.
Hendry, K.R., Robinson, L.F., 2012. The relationship between silicon isotope fractionation in sponges and silicic acid concentration: modern and core-top studies of biogenic opal. Geochim. Cosmochim. Acta 81, 1–12.
Hendry, K.R., Georg, R.B., Rickaby, R.E.M., Robinson, L.F., Halliday, A.N., 2010. Deep ocean nutrients during the Last Glacial Maximum deduced from sponge silicon isotopic compositions. Earth Planet. Sci. Lett. 292, 290–300.
Hendry, K.R., Robinson, L.F., Meredith, M.P., Mulitza, S., Chiessi, C.M., Arz, H., 2012. Abrupt changes in high-latitude nutrient supply to the Atlantic during the last glacial cycle. Geology 40, 123–126.
Hendry, K.R., Robinson, L.F., McManus, J.F., Hays, J.D., 2014. Silicon isotopes indicate enhanced carbon export efficiency in the North Atlantic during deglaciation. Nat. Commun. 5.
Hodson, M.J., Parker, A.G., Leng, M.J., Sloane, H.J., 2008. Silicon, oxygen and carbon isotope composition of wheat (*Triticum aestivum* L.) phytoliths: implications for palaeoecology and archaeology. J. Quat. Sci. 23, 331–339.
Holland, H.D., 2005. Sea level, sediments and the composition of seawater. Am. J. Sci. 305, 220–239.
Horn, M.G., Beucher, C.P., Robinson, R.S., Brzezinski, M.A., 2011. Southern Ocean nitrogen and silicon dynamics during the last deglaciation. Earth Planet. Sci. Lett. 310, 334–339.
Hughes, H.J., Bouillon, S., André, L., Cardinal, D., 2012. The effects of weathering variability and anthropogenic pressures upon silicon cycling in an intertropical watershed (Tana River, Kenya). Chem. Geol. 308–309, 18–25.
Hughes, H.J., Sondag, F., Cocquyt, C., Laraque, A., Pandi, A., Andre, L., Cardinal, D., 2011. Effect of seasonal biogenic silica variations on dissolved silicon fluxes and isotopic signatures in the Congo River. Limnol. Oceanogr. 56, 551–561.
Hughes, H.J., Sondag, F., Santos, R.V., André, L., Cardinal, D., 2013. The riverine silicon isotope composition of the Amazon Basin. Geochim. Cosmochim. Acta 121, 637–651.
Hutchinson, G.E., 1957. A treatise on limnology. Georgraphy, Physics and Chemistry vol. 1. John Wiley & Sons.
Iler, R.K., 1979. Chemistry of Silica — Solubility, Polymerization, Colloid and Surface Properties and Biochemistry. John Wiley & Sons.
Jeandel, C., Oelkers, E.H., 2015. The influence of terrigenous particulate material dissolution on ocean chemistry and global element cycles. Chem. Geol. 395, 50–66.
Jeandel, C., Peucker-Ehrenbrink, B., Jones, M.T., Pearce, C.R., Oelkers, E.H., Godderis, Y., Lacan, F., Aumont, O., Arsouze, T., 2011. Ocean margins: the missing term in oceanic element budgets? EOS Trans. Am. Geophys. Union 92.
Jickells, T.D., An, Z.S., Andersen, K.K., Baker, A.R., Bergametti, G., Brooks, N., Cao, J.J., Boyd, P.W., Duce, R.A., Hunter, K.A., Kawahata, H., Kubilay, N., laRoche, J., Liss, P.S., Mahowald, N., Prospero, J.M., Ridgwell, A.J., Tegen, I., Torres, R., 2005. Global iron connections between desert dust, ocean biogeochemistry, and climate. Science 308, 67–71.
Johannes, R., 1980. Ecological significance of the submarine discharge of groundwater. Mar. Ecol. Prog. Ser. 3, 365–373.
Jones, I.W., Munhoven, G., Tranter, M., Huybrechts, P., Sharp, M.J., 2002. Modelled glacial and non-glacial HCO_3^-, Si and Ge fluxes since the LGM: little potential for impact on

atmospheric CO_2 concentrations and a potential proxy of continental chemical erosion, the marine Ge/Si ratio. Glob. Planet. Chang. 33, 139–153.
Jones, M.T., Gislason, S.R., Burton, K.W., Pearce, C.R., Mavromatis, V., Pogge von Strandmann, P.A.E., Oelkers, E.H., 2014. Quantifying the impact of riverine particulate dissolution in seawater on ocean chemistry. Earth Planet. Sci. Lett. 395, 91–100.
Jones, M.T., Pearce, C.R., Oelkers, E.H., 2012. An experimental study of the interaction of basaltic riverine particulate material and seawater. Geochim. Cosmochim. Acta 77, 108–120.
Jones, M.T., Pearce, C.R., Jeandel, C., Gislason, S.R., Eiriksdottir, E.S., Mavromatis, V., Oelkers, E.H., 2012. Riverine particulate material dissolution as a significant flux of strontium to the oceans. Earth and Planetary Science Letters 355 (356), 51–59.
Kennett, J.P., 1982. Marine Geology. Prentice-Hall, New Jersey (752 pp.).
Kettner, A.J., Syvitski, J.P.M., 2009. Predicting discharge and sediment flux of the Po River, Italy since the Last Glacial Maximum. Analogue and Numerical Modelling of Sedimentary Systems: From Understanding to Prediction. Wiley-Blackwell, pp. 171–189.
Knee, K.L., Paytan, A., 2011. Submarine groundwater discharge: a source of nutrients, metals, and pollutants to the Coastal Ocean. In: Wolanski, E., McLusky, D. (Eds.), Treatise on Estuarine and Coastal Science. Academic Press, Waltham, pp. 205–233.
Köster, J.R., Bol, R., Leng, M.J., Parker, A.G., Sloane, H.J., Ma, J.F., 2009. Effects of active silicon uptake by rice on ^{29}Si fractionation in various plant parts. Rapid Commun. Mass Spectrom. 23, 2398–2402.
Kump, L., Alley, R.B., 1994. Global chemical weathering on glacial time scales. Material Fluxes on the Surface of the Earth, pp. 46–60.
Lambeck, K., Rouby, H., Purcell, A., Sun, Y., Sambridge, M., 2014. Sea level and global ice volumes from the Last Glacial Maximum to the Holocene. Proc. Natl. Acad. Sci. 111, 15296–15303.
Land, M., Ingri, J., Öhlander, B., 1999. Past and present weathering rates in Northern Sweden. Appl. Geochem. 14, 761–774.
Laraque, A., Bricquet, J.P., Pandi, A., Olivry, J.C., 2009. A review of material transport by the Congo River and its tributaries. Hydrol. Process. 23, 3216–3224.
Laruelle, G.G., Roubeix, V., Sferratore, A., Brodherr, B., Ciuffa, D., Conley, D.J., Dürr, H.H., Garnier, J., Lancelot, C., Le Thi Phuong, Q., Meunier, J.D., Meybeck, M., Michalopoulos, P., Moriceau, B., Ní Longphuirt, S., Loucaides, S., Papush, L., Presti, M., Ragueneau, O., Regnier, P., Saccone, L., Slomp, C.P., Spiteri, C., Van Cappellen, P., 2009. Anthropogenic perturbations of the silicon cycle at the global scale: key role of the land-ocean transition. Glob. Biogeochem. Cycles 23, GB4031.
Lauerwald, R., Hartmann, J., Moosdorf, N., Dürr, H.H., Kempe, S., 2013. Retention of dissolved silica within the fluvial system of the conterminous USA. Biogeochemistry 112, 637–659.
Lehtimäki, M., Tallberg, P., Siipola, V., 2013. Seasonal dynamics of amorphous silica in Vantaa River Estuary. SILICON 5, 35–51.
Li, Y., Ding, T., Wan, D., 1995. Experimental study of silicon isotope dynamic fractionation and its application in geology. Chin. J. Geochem. 14, 212–219.
Li, Y.-H., 1988. Denudation rates of the Hawaiian islands by rivers and Groundwaters1. Pac. Sci. 42.
Livingstone, D.A., 1963. Chapter G: chemical composition of rivers and lakes. In: Fleischer, M. (Ed.), Data of Geochemistry. USGS, Washington.
Loucaides, S., Cappellen, P., Roubeix, V., Moriceau, B., Ragueneau, O., 2012. Controls on the recycling and preservation of biogenic silica from biomineralization to burial. SILICON 4, 7–22.
Loucaides, S., Michalopoulos, P., Presti, M., Koning, E., Behrends, T., Van Cappellen, P., 2010. Seawater-mediated interactions between diatomaceous silica and terrigenous sediments: results from long-term incubation experiments. Chem. Geol. 270, 68–79.
Loucaides, S., Van Cappellen, P., Behrends, T., 2008. Dissolution of biogenic silica from land to ocean: role of salinity and pH. Limnol. Oceanogr. 53, 1614–1621.
Lupker, M., France-Lanord, C., Galy, V., Lavé, J., Kudrass, H., 2013. Increasing chemical weathering in the Himalayan system since the Last Glacial Maximum. Earth Planet. Sci. Lett. 365, 243–252.
Mackenzie, F.T., Garrels, R.M., 1966. Chemical mass balance between rivers and oceans. Am. J. Sci. 264, 507–525.
Mackenzie, F.T., Kump, L.R., 1995. Reverse weathering, clay mineral formation, and oceanic element cycles. Science 270, 586–587.
Maier, E., Chapligin, B., Abelmann, A., Gersonde, R., Esper, O., Ren, J., Friedrichsen, H., Meyer, H., Tiedemann, R., 2013. Combined oxygen and silicon isotope analysis of diatom silica from a deglacial subarctic Pacific record. J. Quat. Sci. 28, 571–581.
Maring, H.B., Duce, R.A., 1987. The impact of atmospheric aerosols on trace metal chemistry in open ocean surface seawater, 1. aluminum. Earth Planet. Sci. Lett. 84, 381–392.
Maier, E., Méheust, M., Abelmann, A., Gersonde, R., Chapligin, B., Ren, J., Stein, R., Meyer, H., Tiedemann, R., 2015. Deglacial subarctic Pacific surface water hydrography and nutrient dynamics and links to North Atlantic climate variability and atmospheric CO2. Paleoceanography 30 2014PA002763.
Mariotti, A., Germon, J.C., Hubert, P., Kaiser, P., Letolle, R., Tardieux, A., Tardieux, P., 1981. Experimental determination of nitrogen kinetic isotope fractionation: some principles; illustration for the denitrification and nitrification processes. Plant Soil 62, 413–430.
Martin, J.H., 1990. Glacial–interglacial CO_2 change: the iron hypothesis. Paleoceanography 5, 1–13.
März, C., Meinhardt, A.K., Schnetger, B., Brumsack, H.J., 2015. Silica diagenesis and benthic fluxes in the Arctic Ocean. Mar. Chem. 171, 1–9.
Massey, F.P., Ennos, A.R., Hartley, S.E., 2006. Silica in grasses as a defence against insect herbivores: contrasting effects on folivores and a phloem feeder. J. Anim. Ecol. 75, 595–603.
Matsumoto, K., Sarmiento, J.L., Brzezinski, M.A., 2002. Silicic acid leakage from the Southern Ocean: a possible explanation for glacial atmospheric pCO(2). Glob. Biogeochem. Cycles 16.
Maynard, J.B., 1976. The long-term buffering of the oceans. Geochim. Cosmochim. Acta 40, 1523–1532.
Measures, C., Vink, S., 2000. On the use of dissolved aluminum in surface waters to estimate dust deposition to the ocean. Glob. Biogeochem. Cycles 14, 317–327.
Métivier, Gaudemer, 1999. Stability of output fluxes of large rivers in South and East Asia during the last 2 million years: implications on floodplain processes. Basin Res. 11, 293–303.
Meunier, J.-D., Braun, J.-J., Riotte, J., Kumar, C., Sekhar, M., 2011. Importance of weathering and human perturbations on the riverine transport of Si. Appl. Geochem. 26, S360–S362 (Supplement).
Meybeck, M., Vörösmarty, C., 2005. Fluvial filtering of land-to-ocean fluxes: from natural Holocene variations to Anthropocene. Compt. Rendus Geosci. 337, 107–123.
Michalopoulos, P., Aller, R.C., 1995. Rapid clay mineral formation in Amazon delta sediments — reverse weathering and oceanic elemental cycles. Science 270, 614–617.
Michalopoulos, P., Aller, R.C., 2004. Early diagenesis of biogenic silica in the Amazon delta: alteration, authigenic clay formation, and storage. Geochim. Cosmochim. Acta 68, 1061–1085.
Michalopoulos, P., Aller, R.C., Reeder, R.J., 2000. Conversion of diatoms to clays during early diagenesis in tropical, continental shelf muds. Geology 28, 1095–1098.
Milligan, A.J., Varela, D.E., Brzezinski, M.A., Morel, F., 2004. Dynamics of silicon metabolism and silicon isotopic discrimination in a marine diatom as a function of pCO(2). Limnol. Oceanogr. 49, 322–329.
Milliman, J.D., Boyle, E., 1975. Biological uptake of dissolved silica in the Amazon River estuary. Science 189, 995–997.
Milliman, J.D., Farnsworth, K.L., 2011. River Discharge to the Coastal Ocean: A Global Synthesis. Cambridge University Press, Cambridge.
Milliman, J.D., Meade, R.H., 1983. World-wide delivery of river sediment to the oceans. J. Geol. 91, 1–21.
Mokadem, F., Parkinson, I.J., Hathorne, E.C., Anand, P., Allen, J.T., Burton, K.W., 2015. High-precision radiogenic strontium isotope measurements of the modern and glacial ocean: limits on glacial–interglacial variations in continental weathering. Earth Planet. Sci. Lett. 415, 111–120.
Moore, W.S., 1996. Large groundwater inputs to coastal waters revealed by ^{226}Ra enrichments. Nature 380, 612–614.
Morin, G.P., Vigier, N., Verney-Carron, A., 2015. Enhanced dissolution of basaltic glass in brackish waters: impact on biogeochemical cycles. Earth Planet. Sci. Lett. 417, 1–8.
Muhs, D.R., 2013. The geologic records of dust in the Quaternary. Aeolian Res. 9, 3–48.
Munhoven, G., 2002. Glacial–interglacial changes of continental weathering: estimates of the related CO_2 and HCO_3^- flux variations and their uncertainties. Glob. Planet. Chang. 33, 155–176.
Nelson, D.M., Tréguer, P., Brzezinski, M.A., Leynaert, A., Quéguiner, B., 1995. Production and dissolution of biogenic silica in the ocean: revised global estimates, comparison with regional data and relationship to biogenic sedimentation. Glob. Biogeochem. Cycles 9, 359–372.
Oelkers, E.H., Gislason, S.R., Eiriksdottir, E.S., Jones, M., Pearce, C.R., Jeandel, C., 2011. The role of riverine particulate material on the global cycles of the elements. Appl. Geochem. 26, S365–S369 (Supplement).
Oelze, M., von Blanckenburg, F., Bouchez, J., Hoellen, D., Dietzel, M., 2015. The effect of Al on Si isotope fractionation investigated by silica precipitation experiments. Chem. Geol. 397, 94–105.
Oelze, M., von Blanckenburg, F., Hoellen, D., Dietzel, M., Bouchez, J., 2014. Si stable isotope fractionation during adsorption and the competition between kinetic and equilibrium isotope fractionation: implications for weathering systems. Chem. Geol. 380, 161–171.
Opfergelt, S., Burton, K.W., Pogge von Strandmann, P.A.E., Gislason, S.R., Halliday, A.N., 2013. Riverine silicon isotope variations in glaciated basaltic terrains: implications for the Si delivery to the ocean over glacial–interglacial intervals. Earth Planet. Sci. Lett. 369–370, 211–219.
Opfergelt, S., Cardinal, D., André, L., Delvigne, C., Bremond, L., Delvaux, B., 2010. Variations of δ^{30}Si and Ge/Si with weathering and biogenic input in tropical basaltic ash soils under monoculture. Geochim. Cosmochim. Acta 74, 225–240.
Opfergelt, S., Cardinal, D., Henriet, C., Draye, X., André, L., Delvaux, B., 2006. Silicon isotopic fractionation by banana (*Musa* spp.) grown in a continuous nutrient flow device. Plant Soil 285, 333–345.
Opfergelt, S., de Bournonville, G., Cardinal, D., André, L., Delstanche, S., Delvaux, B., 2009. Impact of soil weathering degree on silicon isotopic fractionation during adsorption onto iron oxides in basaltic ash soils, Cameroon. Geochim. Cosmochim. Acta 73, 7226–7240.
Opfergelt, S., Delmelle, P., 2012. Silicon isotopes and continental weathering processes: assessing controls on Si transfer to the ocean. Compt. Rendus Geosci. 344, 723–738.
Opfergelt, S., Eiriksdottir, E., Burton, K., Einarsson, A., Siebert, C., Gislason, S., Halliday, A., 2011. Quantifying the impact of freshwater diatom productivity on silicon isotopes and silicon fluxes: Lake Myvatn, Iceland. Earth Planet. Sci. Lett. 305, 73–82.
Opfergelt, S., Georg, R.B., Delvaux, B., Cabidoche, Y.M., Burton, K.W., Halliday, A.N., 2012. Silicon isotopes and the tracing of desilication in volcanic soil weathering sequences, Guadeloupe. Chem. Geol. 326–327, 113–122.
Panizzo, V., Crespin, J., Crosta, X., Shemesh, A., Massé, G., Yam, R., Mattielli, N., Cardinal, D., 2014. Sea ice diatom contributions to Holocene nutrient utilization in East Antarctica. Paleoceanography 29, 328–343.
Panizzo, V.N., Swann, G.E.A., Mackay, A.W., Vologina, E., Sturm, M., Pashley, V., Horstwood, M.S.A., 2016. Insights into the transfer of silicon isotopes into the sediment record. Biogeosciences 13, 147–157.

Pastuszak, M., Conley, D.J., Humborg, C., Witek, Z., Sitek, S., 2008. Silicon dynamics in the Oder estuary. Baltic Sea. Journal of Marine Systems 73, 250–262.

Pearce, C.R., Jones, M.T., Oelkers, E.H., Pradoux, C., Jeandel, C., 2013. he effect of particulate dissolution on the neodymium (Nd) isotope and Rare Earth Element (REE) composition of seawater. Earth and Planetary Science Letters 369 (370), 138–147.

Pichevin, L., Reynolds, B., Ganeshram, R., Cacho, I., Pena, L., Keefe, K., Ellam, R., 2009. Enhanced carbon pump inferred from relaxation of nutrient limitation in the glacial ocean. Nature 459, 1114–1117.

Pichevin, L., Ganeshram, R.S., Reynolds, B.C., Prahl, F., Pedersen, T.F., Thunell, R., McClymont, E.L., 2012. Silicic acid biogeochemistry in the Gulf of California: insights from sedimentary Si isotopes. Paleoceanography 27, PA2201.

Picouet, C., Dupré, B., Orange, D., Valladon, M., 2002. Major and trace element geochemistry in the upper Niger river (Mali): physical and chemical weathering rates and CO_2 consumption. Chem. Geol. 185, 93–124.

Pilon-Smits, E.A.H., Quinn, C.F., Tapken, W., Malagoli, M., Schiavon, M., 2009. Physiological functions of beneficial elements. Curr. Opin. Plant Biol. 12, 267–274.

Piperno, D.R., 2001. Phytoliths. In: Smol, J.P., Birks, H.J.B., Last, W.M. (Eds.), Tracking Environmental Change Using Lake SedimentsTerrestrial, Algal and Siliceous Indicators volume 3. Kluwer, London, pp. 235–252.

Pogge von Strandmann, P.A., Burton, K.W., James, R.H., van Calsteren, P., Gíslason, S.R., Mokadem, F., 2006. Riverine behaviour of uranium and lithium isotopes in an actively glaciated basaltic terrain. Earth Planet. Sci. Lett. 251, 134–147.

Pogge von Strandmann, P.A.E., Burton, K.W., James, R.H., van Calsteren, P., Gislason, S.R., Sigfússon, B., 2008. The influence of weathering processes on riverine magnesium isotopes in a basaltic terrain. Earth Planet. Sci. Lett. 276, 187–197.

Pogge von Strandmann, P.A.E., Opfergelt, S., Lai, Y.-J., Sigfússon, B., Gislason, S.R., Burton, K.W., 2012. Lithium, magnesium and silicon isotope behaviour accompanying weathering in a basaltic soil and pore water profile in Iceland. Earth Planet. Sci. Lett. 339–340, 11–23.

Pogge von Strandmann, P.A.E., Porcelli, D., James, R.H., van Calsteren, P., Schaefer, B., Cartwright, I., Reynolds, B.C., Burton, K.W., 2014. Chemical weathering processes in the Great Artesian Basin: evidence from lithium and silicon isotopes. Earth Planet. Sci. Lett. 406, 24–36.

Pokrovsky, O.S., Reynolds, B.C., Prokushkin, A.S., Schott, J., Viers, J., 2013. Silicon isotope variations in Central Siberian rivers during basalt weathering in permafrost-dominated larch forests. Chem. Geol. 355, 103–116.

Presti, M., Michalopoulos, P., 2008. Estimating the contribution of the authigenic mineral component to the long-term reactive silica accumulation on the western shelf of the Mississippi River Delta. Cont. Shelf Res. 28, 823–838.

Prospero, J., Arimoto, R., 2008. Atmospheric transport and deposition of particulate material to the oceans. Encyclopedia of Ocean Sciences, pp. 248–257.

Qin, Y.-C., Weng, H.-X., Jin, H., Chen, J., Tian, R.-X., 2012. Estimation of authigenic alteration of biogenic and reactive silica in Pearl River estuarine sediments using wet-chemical digestion methods. Environ. Earth Sci. 65, 1855–1864.

Quinby-Hunt, M.S., Turehian, K.K., 1983. Distribution of elements in sea water. *EOS* Trans. Am. Geophys. Union 64, 130.

Ragueneau, O., Treguer, P., Leynaert, A., Anderson, R.F., Brzezinski, M.A., DeMaster, D.J., Dugdale, R.C., Dymond, J., Fischer, G., Francois, R., Heinze, C., Maier-Reimer, E., Martin-Jezequel, V., Nelson, D.M., Queguiner, B., 2000. A review of the Si cycle in the modem ocean: recent progress and missing gaps in the application of biogenic opal as a paleoproductivity proxy. Glob. Planet. Chang. 26, 317–365.

Reynolds, B.C., 2009. Modeling the modern marine delta Si-30 distribution. Glob. Biogeochem. Cycles 23.

Reynolds, B.C., Frank, M., Halliday, A.N., 2006. Silicon isotope fractionation during nutrient utilization in the North Pacific. Earth Planet. Sci. Lett. 244, 431–443.

Reynolds, J.H., Verhoogen, J., 1953. Natural variations in the isotopic constitution of silicon. Geochim. Cosmochim. Acta 3, 224–234.

Richter, F.M., Turekian, K.K., 1993. Simple models for the geochemical response of the ocean to climatic and tectonic forcing. Earth Planet. Sci. Lett. 119, 121–131.

Ridgwell, A.J., Watson, A.J., Archer, D.E., 2002. Modeling the response of the oceanic Si inventory to perturbation, and consequences for atmospheric CO_2. Glob. Biogeochem. Cycles 16.

Riebe, C.S., Kirchner, J.W., Finkel, R.C., 2003. Long-term rates of chemical weathering and physical erosion from cosmogenic nuclides and geochemical mass balance. Geochim. Cosmochim. Acta 67, 4411–4427.

Rodellas, V., Garcia-Orellana, J., Masqué, P., Feldman, M., Weinstein, Y., 2015. Submarine groundwater discharge as a major source of nutrients to the Mediterranean Sea. Proc. Natl. Acad. Sci. 12 (13), 3926–3930.

Roerdink, D.L., van den Boorn, S.H., Geilert, S., Vroon, P.Z., van Bergen, M.J., 2015. Experimental constraints on kinetic and equilibrium silicon isotope fractionation during the formation of non-biogenic chert deposits. Chem. Geol. 402, 40–51.

Rudnick, R.L., Gao, S., 2003. 3.01 — Composition of the continental crust. In: Holland, H.D., Turekian, K.K. (Eds.), Treatise on Geochemistry. Pergamon, Oxford, pp. 1–64.

Saccone, L., Conley, D.J., Koning, E., Sauer, D., Sommer, M., Kaczorek, D., Blecker, S.W., Kelly, E.F., 2007. Assessing the extraction and quantification of amorphous silica in soils of forest and grassland ecosystems. Eur. J. Soil Sci. 58, 1446–1459.

Sarmiento, J.L., Gruber, N., 2006. Ocean Biogeochemical Dynamics. PUP, Princeton (503 pp.).

Savage, P.S., Georg, R.B., Williams, H.M., Burton, K.W., Halliday, A.N., 2011. Silicon isotope fractionation during magmatic differentiation. Geochim. Cosmochim. Acta 75, 6124–6139.

Savage, P.S., Georg, R.B., Williams, H.M., Halliday, A.N., 2013. The silicon isotope composition of the upper continental crust. Geochim. Cosmochim. Acta 109, 384–399.

Schopka, H.H., Derry, L.A., 2012. Chemical weathering fluxes from volcanic islands and the importance of groundwater: the Hawaiian example. Earth Planet. Sci. Lett. 339, 67–78.

Schumm, S., 1993. River response to baselevel change: implications for sequence stratigraphy. J. Geol. 279–294.

Sigman, D.M., Boyle, E.A., 2000. Glacial/interglacial variations in atmospheric carbon dioxide. Nature 407, 859–869.

Slomp, C.P., Van Cappellen, P., 2004. Nutrient inputs to the coastal ocean through submarine groundwater discharge: controls and potential impact. J. Hydrol. 295, 64–86.

Sommer, M., Kaczorek, D., Kuzyakov, Y., Breuer, J., 2006. Silicon pools and fluxes in soils and landscapes — a review. J. Plant Nutr. Soil Sci. 169, 310–329.

Staudigel H. 2014. 4.16 — Chemical fluxes from hydrothermal alteration of the oceanic crust. In: H. D. H. K. Turekian (Ed.), Treatise on Geochemistry (Second edition). Elsevier, Oxford, pp. 583–606.

Steinhoefel, G., Breuer, J., von Blanckenburg, F., Horn, I., Kaczorek, D., Sommer, M., 2011. Micrometer silicon isotope diagnostics of soils by UV femtosecond laser ablation. Chem. Geol. 286, 280–289.

Street-Perrott, F.A., Barker, P.A., Leng, M.J., Sloane, H.J., Wooller, M.J., Ficken, K.J., Swain, D.L., 2008. Towards an understanding of late Quaternary variations in the continental biogeochemical cycle of silicon: multi-isotope and sediment-flux data for Lake Rutundu, Mt Kenya, East Africa, since 38 ka BP. J. Quat. Sci. 23, 375–387.

Struyf, E., Conley, D.J., 2012. Emerging understanding of the ecosystem silica filter. Biogeochemistry 107, 9–18.

Struyf, E., Mörth, C.-M., Humborg, C., Conley, D.J., 2010a. An enormous amorphous silica stock in boreal wetlands. J. Geophys. Res. Biogeosci. 115, G04008.

Struyf, E., Smis, A., Van Damme, S., Garnier, J., Govers, G., Van Wesemael, B., Conley, D.J., Batelaan, O., Frot, E., Clymans, W., Vandevenne, F., Lancelot, C., Goos, P., Meire, P., 2010b. Historical land use change has lowered terrestrial silica mobilization. Nat. Commun. 1, 129.

Struyf, E., Smis, A., Van Damme, S., Meire, P., Conley, D., 2009. The global biogeochemical silicon cycle. SILICON 1, 207–213.

Sun, X., Andersson, P., Humborg, C., Gustafsson, B., Conley, D.J., Crill, P., Mörth, C.-M., 2011. Climate dependent diatom production is preserved in biogenic Si isotope signatures. Biogeosciences 8, 3491–3499.

Sun, X., Andersson, P.S., Humborg, C., Pastuszak, M., Mörth, C.-M., 2013. Silicon isotope enrichment in diatoms during nutrient-limited blooms in a eutrophied river system. J. Geochem. Explor. 132, 173–180.

Sun, X., Olofsson, M., Andersson, P.S., Fry, B., Legrand, C., Humborg, C., Mörth, C.-M., 2014. Effects of growth and dissolution on the fractionation of silicon isotopes by estuarine diatoms. Geochim. Cosmochim. Acta 130, 156–166.

Sutton, J.N., Ellwood, M.J., Maher, W.A., Croot, P.L., 2010. Oceanic distribution of inorganic germanium relative to silicon: germanium discrimination by diatoms. Glob. Biogeochem. Cycles 24.

Sutton, J.N., Varela, D.E., Brzezinski, M.A., Beucher, C.P., 2013. Species-dependent silicon isotope fractionation by marine diatoms. Geochim. Cosmochim. Acta 104, 300–309.

Sutton, J.N., 2011. Germanium/silicon and silicon isotope fractionation by marine diatoms and sponges and utility as tracers of silicic acid utilization. Australian National University.

Swann, G.E.A., Leng, M.J., Juschus, O., Melles, M., Brigham-Grette, J., Sloane, H.J., 2010. A combined oxygen and silicon diatom isotope record of Late Quaternary change in Lake El'gygytgyn, North East Siberia. Quat. Sci. Rev. 29, 774–786.

Syvitski, J.P.M., Vorosmarty, C.J., Kettner, A.J., Green, P., 2005. Impact of humans on the flux of terrestrial sediment to the global coastal ocean. Science 308, 376–380.

Taniguchi, M., Burnett, W.C., Cable, J.E., Turner, J.V., 2002. Investigation of submarine groundwater discharge. Hydrol. Process. 16, 2115–2129.

Tegen, I., Kohfeld, K.E., 2006. Atmospheric transport of silicon. SCOPE 66, 81.

Tranter, M., 2005. Geochemical weathering in glacial and proglacial environments. In: Drever, J.I. (Ed.), Surface and Ground Water, Weathering, and Soils. Elsevier, London, pp. 189–205.

Tréguer, P., Nelson, D.M., Vanbennekom, A.J., DeMaster, D.J., Leynaert, A., Queguiner, B., 1995. The silica balance in the world ocean — a reestimate. Science 268, 375–379.

Tréguer, P.J., De La Rocha, C.L., 2013. The world ocean silica cycle. Annu. Rev. Mar. Sci. 5.

Upton, P., Kettner, A.J., Gomez, B., Orpin, A.R., Litchfield, N., Page, M.J., 2013. Simulating post-LGM riverine fluxes to the coastal zone: the Waipaoa River system, New Zealand. Comput. Geosci. 53, 48–57.

Vance, D., Teagle, D.A.H., Foster, G.L., 2009. Variable quaternary chemical weathering fluxes and imbalances in marine geochemical budgets. Nature 458, 493–496.

Vandevenne, F.I., Delvaux, C., Hughes, H.J., André, L., Ronchi, B., Clymans, W., Barão, L., Cornelis, J.-T., Govers, G., Meire, P., Struyf, E., 2015. Landscape cultivation alters δ^{30}Si signature in terrestrial ecosystems. Sci. Rep. 5.

Varela, D.E., Pride, C.J., Brzezinski, M.A., 2004. Biological fractionation of silicon isotopes in Southern Ocean surface waters. Glob. Biogeochem. Cycles 18.

Viers, J., Dupre, B., Gaillardet, J., 2009. Chemical composition of suspended sediments in world rivers: new insights from a new database. Sci. Total Environ. 407, 853–868.

Vigier, N., Burton, K.W., Gislason, S.R., Rogers, N.W., Duchene, S., Thomas, L., Hodge, E., Schaefer, B., 2006. The relationship between riverine U-series disequilibria and erosion rates in a basaltic terrain. Earth Planet. Sci. Lett. 249, 258–273.

von Blanckenburg, F., Bouchez, J., Ibarra, D.E., Maher, K., 2015. Stable runoff and weathering fluxes into the oceans over Quaternary climate cycles. Nat. Geosci. 8, 538–542.

Wadham, J.L., Tranter, M., Skidmore, M., Hodson, A.J., Priscu, J., Lyons, W.B., Sharp, M., Wynn, P., Jackson, M., 2010. Biogeochemical weathering under ice: size matters. Glob. Biogeochem. Cycles 24, GB3025.

Walker, J.C.G., Hays, P.B., Kasting, J.F., 1981. A negative feedback mechanism for the long-term stabilization of Earth's surface-temperature. J. Geophys. Res. Oceans Atmos. 86, 9776–9782.

Weinstein, Y., Yechieli, Y., Shalem, Y., Burnett, W.C., Swarzenski, P.W., Herut, B., 2011. What is the role of fresh groundwater and recirculated seawater in conveying nutrients to the Coastal Ocean? Environ. Sci. Technol. 45, 5195–5200.

Weiss, A., De La Rocha, C., Amann, T., Hartmann, J., 2015. Silicon isotope composition of dissolved silica in surface waters of the Elbe Estuary and its tidal marshes. Biogeochemistry 1–19.
West, A.J., Galy, A., Bickle, M., 2005. Tectonic and climatic controls on silicate weathering. Earth Planet. Sci. Lett. 235, 211–228.
Wetzel, F., de Souza, G.F., Reynolds, B.C., 2014. What controls silicon isotope fractionation during dissolution of diatom opal? Geochim. Cosmochim. Acta 131, 128–137.
White, A.F., Schulz, M.S., Stonestrom, D.A., Vivit, D.V., Fitzpatrick, J., Bullen, T.D., Maher, K., Blum, A.E., 2009. Chemical weathering of a marine terrace chronosequence, Santa Cruz, California. Part II: Solute profiles, gradients and the comparisons of contemporary and long-term weathering rates. Geochim. Cosmochim. Acta 73, 2769–2803.
White, A.F., Vivit, D.V., Schulz, M.S., Bullen, T.D., Evett, R.R., Aagarwal, J., 2012. Biogenic and pedogenic controls on Si distributions and cycling in grasslands of the Santa Cruz soil chronosequence, California. Geochim. Cosmochim. Acta 94, 72–94.
Wille, M., Sutton, J., Ellwood, M.J., Sambridge, M., Maher, W., Eggins, S., Kelly, M., 2010. Silicon isotopic fractionation in marine sponges: a new model for understanding silicon isotopic variations in sponges. Earth Planet. Sci. Lett. 292, 281–289.
Wischmeyer, A.G., De La Rocha, C.L., Maier-Reimer, E., Wolf-Gladrow, D.A., 2003. Control mechanisms for the oceanic distribution of silicon isotopes. Glob. Biogeochem. Cycles 17.
Wolery, T.J., Sleep, N.H., 1976. Hydrothermal circulation and geochemical flux at mid-ocean ridges. J. Geol. 249–275.
Wollast, R., Mackenzie, F.T., 1983. The Global Cycle of Silica. In: Aston, S.R. (Ed.), Silicon geochemistry and biochemistry. Academic Press, London, pp. 39–76.
Xiong, Z., Li, T., Algeo, T., Doering, K., Frank, M., Brzezinski, M.A., Chang, F., Opfergelt, S., Crosta, X., Jiang, F., Wan, S., Zhai, B., 2015. The silicon isotope composition of *Ethmodiscus rex* laminated diatom mats from the tropical West Pacific: implications for silicate cycling during the Last Glacial Maximum. Paleoceanography 30 (7), 803–823 (2015PA002793).
Yool, A., Tyrrell, T., 2003. Role of diatoms in regulating the ocean's silicon cycle. Glob. Biogeochem. Cycles 17.
Yool, A., Tyrrell, T., 2005. Implications for the history of Cenozoic opal deposition from a quantitative model. Palaeogeogr. Palaeoclimatol. Palaeoecol. 218, 239–255.
Young, E.D., Galy, A., Nagahara, H., 2002. Kinetic and equilibrium mass-dependent isotope fractionation laws in nature and their geochemical and cosmochemical significance. Geochim. Cosmochim. Acta 66, 1095–1104.
Zambardi, T., Poitrasson, F., Corgne, A., Méheut, M., Quitté, G., Anand, M., 2013. Silicon isotope variations in the inner solar system: implications for planetary formation, differentiation and composition. Geochim. Cosmochim. Acta 121, 67–83.
Zambardi, T., Poitrasson, F., 2011. Precise Determination of Silicon Isotopes in Silicate Rock Reference Materials by MC-ICP-MS. Geostandards and Geoanalytical Research 35, 89–99.
Ziegler, K., Chadwick, O.A., Brzezinski, M.A., Kelly, E.F., 2005a. Natural variations of $\delta^{30}Si$ ratios during progressive basalt weathering, Hawaiian Islands. Geochim. Cosmochim. Acta 69, 4597–4610.
Ziegler, K., Chadwick, O.A., White, A.F., Brzezinski, M.A., 2005b. $\delta^{30}Si$ systematics in a granitic saprolite, Puerto Rico. Geology 33, 817–820.